Experimental evaporation of hyperacid brines: Effects on chemical composition and chlorine isotope fractionation

Alejandro Rodríguez, Manfred J van Bergen, H.G.M. G M Eggenkamp

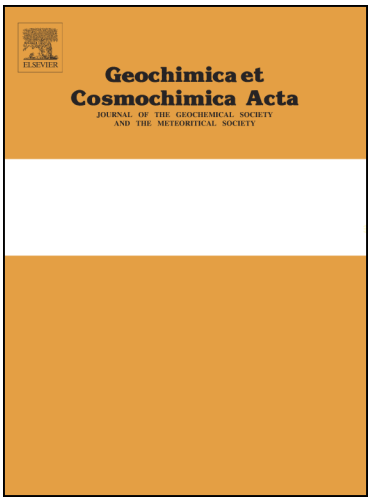

Experimental evaporation of hyperacid brines: Effects on chemical composition and chlorine isotope fractionation

Alejandro Rodríguez, Manfred J. van Bergen, H.G.M. Eggenkamp

PII: S0016-7037(17)30695-6
DOI: https://doi.org/10.1016/j.gca.2017.10.032
Reference: GCA 10537

To appear in: *Geochimica et Cosmochimica Acta*

Received Date: 2 November 2016
Accepted Date: 9 October 2017

Please cite this article as: Rodríguez, A., van Bergen, M.J., Eggenkamp, H.G.M., Experimental evaporation of hyperacid brines: Effects on chemical composition and chlorine isotope fractionation, *Geochimica et Cosmochimica Acta* (2017), doi: https://doi.org/10.1016/j.gca.2017.10.032

EXPERIMENTAL EVAPORATION OF HYPERACID BRINES: EFFECTS ON CHEMICAL COMPOSITION AND CHLORINE ISOTOPE FRACTIONATION

Alejandro Rodríguez and Manfred J. van Bergen:

Utrecht University

Earth Sciences Department

Budapestlaan 4

3508 TA, Utrecht

Netherlands

Nevertheless, it should be indicated on a foot note that my present address is the following:

GFZ German Research Centre for Geosciences

Section 3.1: Inorganic and isotope geochemistry

Telegrafenberg, B458, 14473 Potsdam

email: arodrigu@gfz-potsdam.de<mailto:arodrigu@gfz-potsdam.de>

H.G.M. Eggenkamp:

Institut de Physique du Globe de Paris, Équipe de Géochimie des Isotopes Stables, Sorbonne Paris Cité, UMR 7154, CNRS, 1, rue Jussieu, 75238 Paris Cedex 05, France

Abstract

Hyperacid brines from active volcanic lakes are some of the chemically most complex aqueous solutions on Earth. Their compositions provide valuable insights into processes of elemental transfer from a magma body to the surface and interactions with solid rocks and the atmosphere. This paper describes changes in chemical and $\delta^{37}Cl$ signatures observed in a 1750 hour isothermal evaporation experiment on hyperacid (pH 0.1) sulphate-chloride brine water from the active lake of Kawah Ijen volcano (Indonesia). Although gypsum was the only evaporite

mineral identified in the evolving brine, decreasing Si concentrations may ultimately result in amorphous silica precipitation. Geochemical simulations predict the additional formation of elemental sulphur at lower water activities ($a_{H_2O} \leq 0.65$) that were not reached in the experiment. Absence of other sulphates and halides despite the high load of dissolved elements (initial TDS ca. 100 g/kg) can be attributed to increased solubility of metals, promoted by extensive formation of complexes between the variety of cations and the major anions (HSO_4^-, Cl^-, F^-) present. Chlorine deviations from a conservative behaviour point to losses of gaseous hydrogen chloride ($HCl_{(g)}$) and consequently an increase in Br/Cl ratios.

Chlorine isotope fractionation that accompanied the escape of $HCl_{(g)}$ showed a marked change in sign and magnitude in the course of progressive evaporation of the brine. The calculated factor of fractionation between $HCl_{(g)}$ and dissolved Cl for the initial interval (before 500 hours) is positive ($1000 \ln \alpha_{HCl_{(g)}-Cl_{diss.}} = +1.55 \pm 0.49‰$ to $+ 3.37 \pm 1.11‰$), indicating that, at first, the escaping $HCl_{(g)}$ was isotopically heavier than the dissolved Cl remaining in the brine. Conversely, fractionation shifted to the opposite direction in the subsequent interval ($1000 \ln \alpha_{HCl_{(g)}-Cl_{diss.}} = 5.67 \pm 0.17‰$ to $- 3.97 \pm 0.08‰$), in agreement with values reported in literature. It is proposed that Cl isotopic fractionation in highly acidic brines is controlled by the distribution of dissolved chlorine species, which changes from Cl^- to HCl^0 dominance with the progressive pH decline.

The Kawah Ijen lake acquired its extreme composition through influx of sulphur and halogen-rich magmatic gas components and extensive rock dissolution. If hyperacid brines with comparable chemical composition existed on Mars, evaporation processes up to the extent reported here ($a_{H_2O} = 0.85$), were likely accompanied by losses of gaseous HCl. The resulting changes in Cl isotope compositions, Br/Cl, S/Cl and other ratios in the residual brine might be potentially recorded in assemblages of halogen-bearing secondary evaporation minerals. Also, volcanic-hydrothermal brines as these would extend the stability of liquid water on the Martian surface down to a temperature of -90°C.

1. INTRODUCTION

Many craters hosted by active volcanoes contain SO_4-Cl hyperacid brines, which are complex aqueous solutions from a chemical point of view, being often marked not only by extreme acidity (pH<2) but also by a high load of dissolved components (TDS>2%) (Rowe et al., 1992; Christenson and Wood, 1993; Delmelle and Bernard, 1994; Kempter and Rowe, 2000; Varekamp et al., 2000; 2009; Rouwet el al., 2014). Evaporation is a major process, contributing to an increase in the concentration of total dissolved

components and a decrease of volatile species. Under highly acidic conditions gaseous HCl will escape from the lake surface (Rowe et al. 1992; Rouwet and Ohba, 2015), with volatilization being enhanced by increasing H_2SO_4 abundance (lowering pH), water temperature or Cl- content (Truesdell et al., 1989; Capaccioni et al., 2016).

Limited chlorine isotope data available for acid crater lakes show a modest $\delta^{37}Cl$ range between 0.0 and +1.2‰ (Eggenkamp, 1994; Sharp et al., 2010; Rodríguez et al., 2016a), in which any potential effects from fractionation induced by evaporative loss of gaseous HCl are difficult to deduce. So far, empirical insight into isotopic fractionation between aqueous and gaseous Cl compounds comes from experimental studies, which have been restricted to simple synthetic systems (Sharp et al., 2010). Equilibrium evaporation experiments on 1 M HCl performed by these authors resulted in a chlorine isotope fractionation factor between HCl gas and aqueous chloride ($1000 \ln \alpha_{HCl_{(g)}-Cl^-_{(aq)}}$) of +1.4‰ to +1.8‰ (50-79°C), closely matching theoretical values reported by Schauble et al. (2003) (+1.7‰; 50-100°C) and Czarnacki and Halas (2012) (+1.55‰ to +1.69‰; 60°C). However, Sharp et al. (2010) also conducted evaporation experiments on concentrated hydrochloric acid (11.6 M) in an open system at room temperature, which resulted in a negative value of -4.0‰. They proposed that, in this case, $HCl_{(g)}$ is relatively depleted in ^{37}Cl because the kinetic effect associated with the higher translational velocity of $H^{35}Cl$ predominates over the equilibrium fractionation between $HCl_{(g)}$ and $Cl^-_{(aq)}$ in which ^{37}Cl preferentially partitions into the $HCl_{(g)}$.

This paper extends this experimental work to more complex natural aqueous solutions, and describes the effects of evaporation on the chemical and Cl isotopic composition of SO_4-Cl hyperacid brine from an active volcanic crater lake. The results are potentially relevant for interpretations of the mineralogical marks that fluids have left on the surface of Mars. Firstly, the former presence of SO_4-Cl acidic brines on Mars has been invoked to explain the high concentrations of sulphur and chlorine found by Viking, Pathfinder and MER (Mars Exploration Rovers) Opportunity and Spirit in soils and rock weathering rinds (Brass, 1980; Clark and Van Hart, 1981; Bell et al., 2000; Clark et al., 2005; Tosca and McLennan, 2006; Zolotov and Mironenko, 2007; Schmidt et al., 2008). These findings indicate that probably substantial volcanic degassing of volatile-rich magmas occurred on Mars throughout time (Gellert et al., 2004; Haskin et al., 2005; Gellert et al., 2006). The water-gas-rock interaction processes that once operated at or

near the surface of Martian sulphate-rich terrains may have been similar to those of active terrestrial systems with hyperacid lakes, in view of similarities in alteration mineralogy and element distributions (Rodríguez and van Bergen 2015, Rodríguez et al. 2016b; Rodríguez and van Bergen 2017). The analogy is supported by experimental constraints on the evaporative evolution of acid-sulphate solutions equivalent to those derived from the chemical weathering of synthetic Martian basalt (Tosca and McLennan, 2009). Furthermore, acidic brines are particularly relevant because large amounts of dissolved components could strongly increase the stability of liquid H_2O on Mars by depressing the freezing point and extending its P-T field (Mölhmann and Thompsen, 2011; Elsenousy et al., 2015). Finally, minerals formed as result of evaporation or freezing processes might be an important H_2O-sink on Mars´ surface and could have played a major role in controlling acidity and salinity of Martian paleo-fluids and hence the habitability on this planet (Knauth and Burt, 2002; Toner et al., 2015).

The brine used in the experiment comes from the hyperacid lake of Kawah Ijen, an active andesitic stratovolcano located at the rim of Ijen caldera, the easternmost volcanic complex on Java, Indonesia. This crater lake is one of the world's largest bodies of natural hyperacid brine, and is characterized by a high load of dissolved elements (often >100 g/l), very low pH (<1) and very high concentrations of chlorine (often >20000 mg/kg), sulphate (often >60000 mg/kg) and rock-forming elements Al, Fe, Ca, Mg, Na, K and Si (Delmelle and Bernard, 1994; Delmelle et al., 2000; van Hinsberg et al., 2010; Caudron et al., 2017). The Kawah Ijen lake water type is typically found on active volcanic crater lakes. These waters normally present pH values between 2 and -1, and concentrations of $Cl^-+SO_4^{2-}$ between 3000 and 300000 mg/kg (Varekamp et al., 2000).

2. METHODS

2.1. Evaporation experiment

The Kawah Ijen brine selected for the evaporation experiment was collected on October 30th, 2002 and has been employed as in-house standard for hyperacid brine analysis at the Department of Earth Sciences at Utrecht University. The total amount of brine used for the experiment (1.4 l) was filtered through a 0.2 µm pore size cellulose acetate membrane to remove amorphous silica and gypsum that had precipitated upon storage for many years. A total of 26 plastic Greiner® tubes were filled with approximately 50

ml brine, and were collectively placed on a plastic rack that was partially submerged in a water bath at 60°C (Fig. 1). The initial weight of all samples was recorded before the evaporation experiment started.

The experiment lasted 1750 hours (73 days) during which duplicate samples were removed from the water bath at certain time intervals. Directly after removal, the final weight, pH and electrical conductivity, measured at room temperature (20±1°C), were determined for each sample. Next, six aliquots of approximately 1.6, 0.6 and 0.2 grams were diluted 10, 25 and 100 times with deionised water for IC (ion-chromatography) analysis, and 10, 25 and 100 times with 2% Suprapur® HNO_3 solution for ICP-OES (inductively coupled plasma optical emission spectrometry) analysis. Towards the end of the evaporation experiment, some samples had to be further diluted up to 650 times for IC analysis. The pH and conductivity measurements were performed with a WTW® 3430 portable multimeter at room temperature (20°C). The pH electrode was calibrated with pH 1, 4 and 7 buffers. The conductivity electrode was calibrated with a 0.01 M KCl standard. Both electrodes were calibrated before every measurement. The acicular crystals formed during the experiment where separated from the solutions by filtration through a 0.2 µm pore size cellulose acetate membrane, washed with deionized water and finally dried overnight at 60°C.

2.2. Analytical methods

2.2.1. Major elements

The fluoride concentrations were determined by ion chromatography (IC), using a Dionex® ICS-3000, equipped with a Dionex®IonPac® AS 19 column. A gradient elution of 10 – 50 mM KOH was utilized. Total sulphur (S_T), Cl, Al, B, Br, Ca, Fe, K, Mg, Na, Si, Sr and Ti were analysed by inductively coupled plasma optical emission spectrometry (ICP-OES) with a Spectro® Ciros® instrument. The average relative uncertainties on the analysis where the following: 1% (S_T and Si); 2% (B, Br, Ca, Fe, K, Mg, Na and Sr); 3% (Al and Cl) and 4% (Ti and F). All the aforementioned analyses where carried out at the Department of Earth Sciences, Utrecht University.

2.2.2. Chlorine isotopes

Samples for $\delta^{37}Cl$ analysis were prepared following a variation of the method described by Kaufmann (1984) and Eggenkamp (1994). Based on the Cl concentrations determined by ICP-OES, an aliquot of an undiluted sample from the evaporation experiment was treated with 4 ml of 1 M KNO_3, 1 ml of H_2O_2 (30 wt.%) and 1 ml of concentrated HNO_3 (65 wt.%). Then this mixture was heated to 80°C for 30 minutes before 1 ml of 0.2 M $AgNO_3$ was added. In this way, approximately 10 mg of AgCl were precipitated from each sample and collected after filtering through a Whatman® type GF/F glass fibre and finally dried overnight at 80°C. Subsequently, the AgCl was reacted with iodomethane (CH_3I) in order to form chloromethane (CH_3Cl) at 70 - 80°C during 48 hours in vacuum glass ampoules. The chloromethane was separated from the excess CH_3I by gas chromatography using a 75 cm long, 6.35 mm OD SS column, filled with Porapak® Q 80-100 mesh at 140°C with helium as carrier gas. The analyses of CH_3Cl were carried out on a VG SIRA 24 EM mass spectrometer at the Department of Earth Sciences of Utrecht University. As shown in equation (1), chlorine isotope data are reported as a delta notation ($\delta^{37}Cl$) using a reference sample of sea water from the Atlantic Ocean collected near Madeira in 1982, known as Standard Mean Ocean Chloride or SMOC (Kaufmann, 1984). The analytical accuracy was ±0.16‰ (1σ) based on long-term analyses of this standard. Nevertheless, samples were analysed at least in duplicate and the averages were accepted if the difference between duplicates was ≤0.10‰.

$$\delta^{37}Cl\,(‰) = \frac{\left(^{37}Cl/^{35}Cl\right)_{sample} - \left(^{37}Cl/^{35}Cl\right)_{SMOC}}{\left(^{37}Cl/^{35}Cl\right)_{SMOC}} \times 1000 \qquad (1)$$

2.2.3. Chemical composition of the precipitate

Raman spectra were obtained from the precipitate (acicular crystals) formed during the experiment using a 532 nm wavelength Nd-YAG laser. An optical microscope with a 50 x long working distance objective lens provided a laser spot size of ~2 μm at the sample surface. The scattered light was dispersed using a grating of 600 grooves/mm before being collected on a charge coupled device camera. Each spectrum was acquired 20 times with an integration time of 0.2 seconds. Detailed images were also obtained from carbon-coated crystals with a JEOL JCM-6000 Benchtop SEM. Spot analysis were performed on carbon-coated crystals with a JEOL JXA-8530F field-emission-electron-

microprobe. The beam conditions were 15 kV, 10 nA and 20 μm diameter; scans were also done with a defocused 10 μm beam.

2.3. Geochemical modelling

The geochemical modelling software PHREEQC, version 3.1 (Parkhurst and Appelo, 1999), was used to calculate aqueous species distributions and mineral saturation states. The Lawrence Livermore National Laboratories thermodynamic database (llnl.dat) was used. Additionally, ion interaction parameters from many ion pairs were included (Pitzer and Mayorga, 1973). The pH values at 60°C were recalculated by charge balance with PHREEQC, as it is recommendable for extremely acid waters (Nordstrom et al., 2000).

3. RESULTS

3.1. Evaporation rates

The total duration of the evaporation experiment was 1750 hours (~73 days). The weight loss of the brine virtually stopped after 1340 hours (samples 12 and 13) when a maximum of 58% was reached. (Fig. 2; Table 1). Evaporation rates were calculated taking the transversal area of the Greiner® tubes (0.0601 dm^2) into account. The brine exhibited a decrease in evaporation rates throughout the experiment. In particular, around 400 hours, the brine showed a marked decrease (from 1.01 to 0.83 $g/h/dm^2$), after which there was a smooth decline until the end of the experiment.

3.2. Chemical composition, mineral saturation states and speciation in the brine

The hyperacid SO_4-Cl composition of the Kawah Ijen brine is a result of the condensation of magmatic SO_2, HCl, HF and HBr gases in water of largely meteoric origin. The acidity comes mainly from HSO_4^- dissociation, together with contributions of $HCl_{(aq)}$, $HF_{(aq)}$ and $HBr_{(aq)}$ (Giggenbach, 1975; 1987). Because of the strong acidity, the fluid contains high concentrations of rock-forming elements such as Ca, Al, Fe, Mg, Na, K and Si derived from the dissolution of primary minerals and glass. At the start of the experiments, the initial concentrations of total sulphur (S_T), Cl, F, Br, Al, Fe, K, Na, Ca, and Mg in the brine were 21800, 22100, 1410, 56, 5730, 1970, 1230, 1110, 690 and 690 mg/kg, respectively. Total dissolved solids (TDS) were 96 g/kg and pH was 0.10 (20±1°). At the end of the

experiment, upon 58 wt. % of evaporation, the final concentrations were (in the same order): 52400, 45900, 3110, 124, 13800, 4920, 2920, 2610, 700 and 1630 mg/kg. The total dissolved solids increased up to 234 g/kg, and pH decreased to -0.41 (20±1°) (Table 2).

In order to explore elemental losses by mineral precipitation or evaporation of volatile phases, time series were plotted for ratios of element concentrations against Mg, adopted as a perfectly conservative solute (Fig. 3). Notable negative deviations from a horizontal trend in the ratio plots indicate removal of Cl, Ca, Sr and Si during some intervals in the evaporation process. The Cl/Mg ratio shows a steady decline virtually from the start (Fig. 3a), indicating an escape of gaseous HCl from the brine throughout the experiment, in absence of a Cl-bearing precipitating solid phase. There is a concomitant gradual increase of log f_{HCl} values in the course of the experiment (Fig. 4a). Conversely, the Br/Mg ratio remains largely constant although a decreasing tendency is suggested for the starting interval (Fig. 3b). The increase of log f_{HBr} values was relatively small (Fig. 4a).

The Ca depletion in the brine after 594 hours (Fig. 3c) coincides with the appearance of acicular crystals from sample 10 (762 hours) onward until the end of the experiment. According to Raman spectra and electron backscatter imaging (Figs. 5a and 5b), together with semi-quantitative EPMA-WDS analysis this phase is gypsum ($CaSO_4 \cdot 2H_2O$), containing appreciable amounts of Sr (average 700±200ppm). The decrease of the Sr/Mg follows the same timing as that of Ca/Mg (Fig. 3c). Hence, precipitation of gypsum explains the gradual depletion of both Ca and Sr, since the latter can substitute Ca (Ichikuni and Musha, 1978; Kushnir, 1980). Celestine ($SrSO_4$) was not detected and remained far from saturation (Fig. 4b).

Silicon concentrations exhibit a significant decrease towards the end of the experiment as is expressed in the Si/Mg decline after 930 hours (Fig. 3d). Because no silica-bearing solid phase was directly detected by SEM analyses, it is conceivable that escape of gaseous $SiF_{4(g)}$ could be responsible for the Si loss. However, this option is difficult to substantiate with the F/Mg trend, from which no obvious loss of fluorine can be deduced (Fig. 3b). On the other hand, it must be realized that the fluorine required to match the loss of silicon as $SiF_{4(g)}$ is too little, compared to the amount of dissolved F (>1410

mg/kg), to be noticeable within the analytical error. Alternatively, the apparent Si loss resulted from the precipitation of amorphous silica particles, which remained unobserved because of their small size and quantity (see Discussion). Other element/Mg ratios display horizontal trends (Figs. 3e and 3f), suggesting a conservative behaviour.

As Figure 4b illustrates, Ca-sulphates and amorphous silica were the only major-element hosts that approached saturation closest in the PHREEQC models. Calculated fugacities of $HCl_{(g)}$, $HBr_{(g)}$ and $SiF_{4(g)}$ show increases with time (Fig. 4a). The behaviour of Ti is governed by anatase (TiO_2), which is commonly saturated in the Kawah Ijen lake (Delmelle and Bernard, 1994; Delmelle et al., 2000). During the experiment, the concentrations of dissolved Ti were close to equilibrium (Figs. 3f and 4b), taking analytical uncertainty into account. Fluorite (CaF_2), cryolite (AlF_3) and halite (NaCl) remained always well undersaturated, showing an initial increase in saturation indices (SI), followed by a levelling off (Fig. a, Supplementary Electronic Annex EA-1). Iron and magnesium sulphates remained undersaturated throughout the experiment. The saturation indices of szolmolnokite ($FeSO_4 \cdot H_2O$), rozenite ($FeSO_4 \cdot 4H_2O$), siderotile ($FeSO_4 \cdot 5H_2O$), ferrohexahydrite ($FeSO_4 \cdot 6H_2O$) and melanterite ($FeSO_4 \cdot 7H_2O$) show an initial increase, then a decline and finally an increase again towards the end of the experiment (Fig. b, EA-1). The SI values of kieserite ($MgSO_4 \cdot H_2O$), starkeyite ($MgSO_4 \cdot 4H_2O$), pentahydrite ($MgSO_4 \cdot 5H_2O$), hexahydrite ($MgSO_4 \cdot 6H_2O$) and epsomite ($MgSO_4 \cdot 7H_2O$) increased steadily with time (Fig. c, EA-1).

In summary, the only phases that formed upon brine evaporation were $HCl_{(g)}$, gypsum and a Si-bearing phase (probably amorphous SiO_2). Anatase (TiO_2) was in equilibrium and its presence could not be detected by the analysis.

Total dissolved chlorine ($Cl_{diss.}$) is present in the form of undissociated hydrogen chloride (HCl^0) and Cl^-, with the activity of the latter species being dominant (Fig. 6). When evaporation proceeded, the activity of HCl^0 increased strongly, reflecting displacement of the equilibrium of reaction (2) to the left hand side due to the increase of H_3O^+. The same mechanism favoured the formation of $H_2SO_4^0$ and HBr^0, but activities of these species were several orders of magnitude lower than that of HCl^0 (reactions 3 and 4) (Fig. 6).

$$HCl^0 + H_2O \Leftrightarrow Cl^- + H_3O^+ \quad (2)$$

$$H_2SO_4 + H_2O \Leftrightarrow HSO_4^- + H_3O^+ \quad (3)$$

$$HBr^0 + H_2O \Leftrightarrow Br^- + H_3O^+ \quad (4)$$

Aluminium has a strong tendency to form complexes with F^-, so that most of this element is present as AlF_2^+, AlF^{2+} and AlF_3 (Fig. a, EA-2). On the other hand, Fe^{2+} and Fe^{3+} are predominantly complexed with Cl^-, forming $FeCl^+$ and $FeCl^{2+}$, respectively (Figs. b and c; EA-2). It should be mentioned that, due to the extreme acidity of the Kawah Ijen brine, iron is predominantly in its lower oxidation state (Fe^{2+}). Magnesium and calcium are mainly present as Mg^{2+} and Ca^{2+}, respectively, but also form complexes with SO_4^{2-} and Cl^- such as $MgCl^+$, $MgSO_4^0$, $CaCl^+$ and $CaSO_4^0$, where the sulphur-bearing species always have higher activities than their chlorine-bearing counterparts (Figs. d and e; EA-2). Finally, potassium and sodium tend to remain largely as K^+ and Na^+, with the most significant complexes being $KHSO_4^0$ and $NaCl^0$, respectively (Figs. f and g; EA-2). The dominant strontium species in the early part of the experiment was Sr^{2+}, which decreased rapidly in favour of the $SrCl^+$ and $SrSO_4^0$ complexes (Figure h, EA-2). The apparent strong reduction of Sr^{2+} availability in the course of the experiment may explain our observation that the precipitated gypsum incorporated 3-4 times less strontium than expected from low-temperature gypsum-solution partitioning data (Ichikuni and Musha, 1978; Kushnir, 1980).

3.3. Chlorine isotope trends and Cl losses

From the initial $\delta^{37}Cl$ composition of the hyperacid brine (+0.36±0.05‰) until sample 9 (500 hours), a slight decrease down to +0.22±0.04‰ was observed. This trend was followed by a significant increase up to +0.68±0.05‰ in the last sample (Table 3, Fig. 7). The changes in isotope composition are accompanied by chlorine losses through escaping $HCl_{(g)}$, given the absence of any solid precipitating Cl-bearing phase during the experiment. The $HCl_{(g)}$ degassing of the brines probably started early (Fig. 3a), but the significant increase in log f_{HCl} values after 500 hours (Fig. 4a) suggests an enhancement from that moment on.

Chlorine losses by degassing $HCl_{(g)}$ were calculated from the differences between measured and calculated Cl concentrations (Table 3). The concentration differences

were transformed into mass losses (mg) for each sample, based on the remaining liquid mass (Table 1). Fractionation between $HCl_{(g)}$ and total dissolved chlorine ($Cl_{diss.}$) during the evaporation experiment can be calculated using the Rayleigh fractionation model:

$$\delta_f - \delta_i = (1000 + \delta_i)(F^{(\propto -1)} - 1) \quad (5)$$

Where δ_i and δ_f are the $\delta^{37}Cl$ composition for the initial Kawah Ijen brine (+0.36±0.05‰; sample t=0) and the subsequent $\delta^{37}Cl$ compositions throughout the evaporation experiment, respectively. The fractionation factor is α, and F is the total chlorine remaining in the liquid, defined by:

$$F = \frac{Cl_{final}(mg)}{Cl_{initial}(mg)} \quad (6)$$

Expressing equation (5) in a linear form gives:

$$ln\left(\frac{\delta_f + 1000}{\delta_i + 1000}\right) = (\alpha - 1)F \quad (7)$$

Where α can be obtained from the slope of the line. The experiments yielded two distinctive trends for different time intervals (Table 3). The corresponding $\alpha_{HCl_g - Cl_{diss.}}$ values are 1.00300±0.000002 (t=0-500 hours) and 0.994479±0.000004 (t=500-1750 hours) (Fig 8a). The fractionation factors ($1000 \ln \alpha_{HCl_g - Cl_{diss.}}$) before and after 500 hours, are +2.963±0.014‰ and -5.536±0.004‰, respectively (Fig 9a). This implies that the $HCl_{(g)}$ produced during the first 500 hours of the experiment was enriched in ^{37}Cl compared to the $Cl_{diss.}$ in the hyperacid brine, whereas after 500 hours it was depleted in ^{37}Cl.

An alternative approach to calculate these fractionation factors is by using *F* values derived from the ratio between Cl and a conservative element such as boron. For each sample, the Cl/B ratio was determined and normalized to the ratio in the initial brine (sample t=0). In this case:

$$Cl_{final}(mg) = Cl_{initial}(mg)\left(\frac{Cl_{final}/B_{final}}{Cl_{initial}/B_{initial}}\right) \quad (8)$$

and then,

$$Cl_{initial}(mg) - Cl_{final}(mg) = Cl_{loss} = HCl_{(g)} \quad (9)$$

The resulting *F* values and fractionation factors were again obtained from equations (6) and (7) by linear regression, assuming Rayleigh fractionation (EA-3) (Figs. 8b and 9b). In a similar way, *F* values and fractionation factors were also calculated for Fe and Mg as conservative elements (EA-3), (Figs. 8c, 8d, 9c and 9d) and essentially the same results were obtained (Table 4).

4. DISCUSSION

According to experiments and models reported in literature, calcium sulphates are often the first phases to precipitate upon evaporation of saline brine waters, followed by a variety of K, Mg, Fe^{2+} and Fe^{3+}-sulphates (Tosca and McLennan, 2006; 2009; Gamazo et al., 2011; Elsenousy et al., 2015; Toner et al., 2015). In evaporation experiments on a Cl-bearing acid-sulphate fluid with a composition derived from chemical weathering of a synthetic olivine-bearing Martian basalt, Tosca and McLennan (2009) found gypsum, Mg-rich voltaite, an unidentified (Mg,Fe)-sulphate-heptahydrate and rhomboclase as precipitating minerals. The concomitant changes in solution chemistry were first a loss of Ca and a further depletion of K, Al, Fe, Mg and SO_4 towards the end of the run when most of H_2O was evaporated. No detectable fractionation of Cl occurred. The authors inferred that sulphate mineralogy and chemical evolution of the solution did not follow an equilibrium pathway predicted by thermodynamic models but were influenced by kinetic controls on the precipitation of copiapite-group minerals. Gamazo et al. (2011) modelled the evaporation of Mg-Na-Cl-SO_4 brine water from Quero lake (Spain), and observed the appearance of an anhydrite-gypsum paragenesis at a_{H_2O} = 0.78, followed by epsomite-hexahydrite and hexahydrite-kieserite paragenesis at a_{H_2O} values of 0.57 and 0.50, respectively. Similarly, based on the Na-K-Ca-Mg-Cl-SO_4-ClO_4 brines that could have produced the salt assemblages at the Phoenix landing site on Mars, the evaporation models of Toner et al. (2015) predicted the appearance of anhydrite-gypsum, epsomite-hexahydrite and hexahydrite-kieserite paragenesis at a_{H_2O} values of 0.68, 0.56 and 0.52, respectively.

In comparison to this general picture, two outcomes of our evaporation experiment regarding the formation of new phases during evolution of the brine are noticeable: the small number of precipitating minerals despite the high load and diversity of dissolved elements, and the apparent escape of several volatile components other than water.

Relative to the evaporative enrichment factor $\left(EF = \frac{final\ concentration}{initial\ concentration}\right)$ of a perfectly conservative element such as Mg (2.37), the EF values of Ca (1.01), Si (1.72), Sr (1.97) and Cl (2.08) are significantly lower, indicating partial removal of these elements into phases, inferred to be gaseous HCl (for Cl) and gypsum (for Ca and Sr) and possibly amorphous silica (for Si) as solids. Due to its elevated concentration in the brine, the total sulphur loss associated with gypsum formation was too little to be measurable outside the analytical error.

4.1. Hyperacid brine evolution and evaporite minerals

The observation that gypsum and possibly amorphous silica were the only precipitating phases in the course of the experiment is grossly consistent with thermodynamic equilibrium, since the models indicate that other phases stayed far from saturation (Fig. 4b). Gypsum was the precipitating calcium-sulphate although anhydrite tended to be closer to saturation. Reported temperatures of 42-60°C for the transition between gypsum and anhydrite (Posnjak 1938; 1940; Hardie, 1967; Innorta et al., 1980) encompass our 60°C experimental temperature. Also, the transition temperature depends on overall solution chemistry and water activity (Farrah et al., 2004; Li and Demopoulos, 2006; Azimi et al., 2007). A plausible explanation for the appearance of gypsum instead of anhydrite is a kinetic control. Since the nucleation rate of anhydrite is considerably slower, gypsum might remain as a metastable phase up to 120°C (Ostroff, 1964; Freyer and Voigt, 2003; Azimi and Papangelakis, 2011; Ossorio et al., 2014).

In absence of unambiguous evidence for fluorine loss, which would support possible degassing of $SiF_{4(g)}$, we tentatively attribute the concentration decline of Si to formation of amorphous silica, a phase that is commonly saturated in the Kawah Ijen lake (Delmelle and Bernard, 1994; Delmelle et al., 2000). However, because the brine sample had been filtered and the experimental temperature was some 20°C higher than during its storage, the solution must have been undersaturated at least at the start of the experiment. Similar to gypsum, the PHREEQC models do not predict attainment of saturation for amorphous silica (Fig. 4b) but its SI value reached a maximum approximately at the time when the Si concentration decrease started (cf. Fig. 3d). Calculations based on Gunnarsson and Arnórsson (2000) suggest that $SiO_{2_{am.}}$ solubility at 60°C would be almost three times the maximum concentration measured in the

experiment, but the temperature equations of these authors describe the solubility in pure water, making its applicability to the hyperacid highly saline brine questionable. We speculate that nanoparticles did form under the extreme acidic conditions and eventually reached a sufficiently large size to be filtered out, since increasing ionic strength, decreasing water activity and decreasing pH suppress amorphous silica solubility and promote polymerization and particle flocculation rates (Marshall and Warakomski, 1980; Gorrepati et al., 2010).

In order to explore the possible stability of phases beyond the lowest water activity reached in the experiments (a_{H_2O} = 0.85), an evaporation process was simulated in PHREEQC, whereby one litre of Kawah Ijen brine with the same composition as the starting experimental sample was evaporated by removing water in 1000 steps at 60°C. The run did not converge after the 990th step, when 99% (985 g) of the initial water content was removed and the ionic strength of the brine reached 163 m. The a_{H_2O} values dropped from 0.95 to 0.32. The only phases formed were hydrogen chloride ($a_{H_2O} \leq$ 0.86), gypsum ($a_{H_2O} \leq 0.83$) and elemental sulphur ($a_{H_2O} \leq 0.65$) (Figs. 10a and 10b). At the end of the simulation szolmolnokite ($FeSO_4 \cdot H_2O$) and rozenite ($FeSO_4 \cdot 4H_2O$) together with kieserite ($MgSO_4 \cdot H_2O$) and starkeyite ($MgSO_4 \cdot 4H_2O$) were among the iron and magnesium sulphates that approached the highest saturation levels, but none of these salts were predicted to precipitate, even at the lowest a_{H_2O} values of the simulation. The same applied for some halides as well (Figs. a, b and c; EA-4).

Considering these observations, the absence of precipitating halide and sulphate phases other than gypsum in the course of the experiment is largely in line with equilibrium modelling results. Apparently, the elevated concentrations reached by Cl and S_T (total sulphur) promoted complexation with Mg and Fe, mainly as $FeCl^+$, $FeCl^{2+}$, $FeSO_4^0$, $MgCl^+$ and $MgSO_4^0$, which increased the solubilities of these cations and prevented them from precipitating as salts (Figs. 6, 11 and EA-2, EA-5). Similar arguments explain the absence of Al-, K- or Na-bearing phases. Our experimental and theoretical findings are also consistent with field evidence, since gypsum is usually the only major sulphate found in volcanic lake settings where hyperacid brine is subjected to simple evaporation alone (e.g., Rodríguez et al. 2016b; Rodríguez and van Bergen 2017). Amorphous silica is also a common phase in these surface expressions of volcanic-hydrothermal systems, where

its precipitation is largely governed by a drop of the brine temperature under ambient conditions.

4.2. Hyperacid brine evolution and volatile phases

The progressive water loss and concomitant pH decline not only caused an overall elemental concentration increase, but according to equation (2), it also promoted the formation of $HCl_{(aq)}$ at the expense of Cl^-. The Br/Cl ratios increased slightly (Fig. 12) due to stronger volatilization of $HCl_{(g)}$ than $HBr_{(g)}$, since in aqueous solutions $HBr_{(ac)}$ is a stronger acid than $HCl_{(ac)}$ and thus tends to remain dissociated to a larger extent (Marcus, 1979). The model predicts that Br/Cl ratios become even more pronounced at higher degrees of evaporation than covered by our experiment, with molar Br/Cl ratios in the remaining solution ultimately increasing up to more than 30 times the starting value. A simultaneous increase in the S_T/Cl ratio further confirms the $HCl_{(g)}$ loss (Fig. 12). Both the experimental and modelling results thus provide evidence for unequal rates of halogen volatilization from highly acidic solutions as an efficient mechanism to fractionate Cl from Br, two elements that commonly show a similar hydrophilic behaviour in most terrestrial environments (Aiuppa et al., 2009).

Complexities in the partitioning behaviour of Cl and Br among co-existing brine and vapour have also been highlighted in studies of phase separation in sub seafloor hydrothermal systems. Results from field studies and autoclave experiments are not conclusive as to whether Br or Cl preferentially partitions into the low-salinity vapour phase fluids relative to the brines. Although most experiments and measurements on natural vent fluids tend to favour preferential partitioning of Br in the vapour phase (e.g., Von Damm et al., 2003; Foustoukos and Seyfried, 2007; Seo and Zajacz, 2016), others reported an opposite trend (e.g., Liebscher et al., 2006). Factors that may influence the partitioning behaviour include P-T conditions at which phase separation occurs, density contrast between vapour and brine, and alkali metals present in the solution (Seo and Zajacz, 2016).

4.3. Chlorine isotope fractionation – changing mechanism during evaporation

Theoretical equilibrium $1000 \ln \alpha_{HCl_{(g)}-Cl_{diss.}}$ values at 60°C reported by Czarnacki and Halas (2012) are +1.55‰ and +1.69‰, based on data from Urey and Greiff (1935) and

Schauble et al. (2003), respectively. Experimental results of Sharp et al. (2010) for equilibrium Cl isotope fractionation between $HCl_{(g)}$ and hydrochloric acid are +1.4 to +1.8‰ between 50 and 79°C. These authors attributed the preference of the heavy Cl isotope for the gas phase to the differences in bond types, because the bond between Cl and H in the $HCl_{(g)}$ molecule will be stronger than that of a solvated Cl^- ion in an aqueous solution and therefore more capable to hold the heavier ^{37}Cl.

Our experimental results before 500 hours are consistent with the tendency that ^{37}Cl preferentially escapes in the evaporating $HCl_{(g)}$. However, the magnitude of fractionation is higher (average of four estimates is +2.5‰, Table 7), although for one approach (Cl mass losses based on B/Cl ratios) the result of +1.55±0.49‰ is closer to the theoretical values of Czarnacki and Halas (2012). This enhanced isotopic fractionation effect can be explained by the experimental conditions of open-system evaporation, instead of the closed-system equilibrium cases on which the previous theoretical and experimental results were based.

In contrast, the experimental results after 500 hours point to a fractionation in opposite direction, i.e. with a strong preference of light ^{35}Cl for the gas phase (average of four estimates is -4.9‰, Table 4). Sharp et al. (2010) found a similar partitioning behaviour in a kinetic evaporation experiment with concentrated hydrochloric acid (11.6 M) at room temperature, which yielded a $1000 \ln \alpha_{HCl_{(g)}-Cl_{diss.}}$ value of -4.0‰. They ascribed this to a kinetic effect associated with the higher translational velocity of $H^{35}Cl$, which will thus escape more readily from the solution.

The change in overall fractionation behaviour in the course of the evaporation experiment can be explained by individual fractionation steps during the two successive reactions needed to form gaseous $HCl_{(g)}$ from the solution:

$$Cl^- + H_3O^+ \Leftrightarrow HCl^0 + H_2O \quad (10)$$

$$HCl^0 \Leftrightarrow HCl_{(g)} \quad (11)$$

The formation of aqueous HCl^0 (reaction 10) is associated with a positive fractionation factor, and the evaporation step (reaction 11) with a negative one. Competition between these opposing effects thus determines the sign and magnitude of the overall isotopic fraction between gaseous $HCl_{(g)}$ and total dissolved Cl.

According to our speciation calculations, Cl^- was the dominant Cl species in solution before 500 hours (80.5% of the total chlorine molality at t=0 hours, Fig. 13), which suggests that reaction (10) was the rate limiting step in the formation of $HCl_{(g)}$. Apparently, the effect of the associated isotopic fractionation overwhelmed that of the subsequent evaporation step, so that the first escaping hydrogen chloride consisted mainly of $H^{37}Cl_{(g)}$. After 500 hours, HCl^0 became the dominant species (60.5% at t=1750 hours, Fig. 12), which turned kinetic fractionation accompanying reaction (11) into the determining factor. Hence, as soon as much of the chlorine in the solution was converted into HCl^0, the bonding effect became less important in fractionating the isotopes during $HCl_{(g)}$ evaporation in comparison to the kinetic effect associated with translational velocity differences between $H^{35}Cl^0$ and $H^{37}Cl^0$. Consequently, from then on, hydrogen chloride preferentially escaped as $H^{35}Cl_{(g)}$. According to PHREEQC calculations, at 25°C, HCl^0 accounts for 63.1% of the total chlorine concentration, and 36.9% for Cl^- in a concentrated hydrochloric acid solution, which implies that the kinetic evaporation experiments of Sharp et al. (2010) mainly measured the fractionation between HCl^0 and $HCl_{(g)}$ as a product of reaction (11), similar to the conditions in our experiment after 500 hours. The correspondence in sign and magnitude of the isotopic fractionation between the two experiments supports this conjecture.

Following this reasoning, the apparent fractionation of chlorine isotopes between gaseous HCl and total Cl in an aqueous solution depends on the speciation of dissolved Cl, i.e. on the proportions of Cl^- and HCl^0. As the speciation calculations demonstrate, the experimental brine may also contain substantial amounts (up to 25%) of various complexed Cl species (Fig. 12). Because fractionation factors among all these dissolved species are unknown, a rigorous quantitative approach is not feasible, so that the inferred magnitudes for the initial and final parts of the experiment should be taken as approximations for the two different fractionation regimes. Further experimental and theoretical work is needed to substantiate these findings and to clarify the underlying controls.

4.4. Implications for Cl isotope signatures of volcanic crater lakes

The Cl isotope signature of hydrothermal fluids that feed an active volcanic lake is initially determined by the source(s) of chlorine, commonly a shallow magma body undergoing exsolution, and potentially also by fractionation during subsequent

subsurface rock-gas-liquid interactions in the hydrothermal system or by a mixture of chlorine from shallow reservoirs such as seawater, groundwater or evaporites (Li et al., 2015; Rodríguez et al., 2016a). Field observations revealed that gaseous HCl occasionally escapes from the surface of warm, highly acidic volcanic lakes (Rowe et al. 1992; Rouwet and Ohba, 2015; Rouwet et al., 2016; Rodríguez et al., 2016a), with volatilization being enhanced by increasing H_2SO_4 abundance (lowering pH), water temperature or Cl^- content (Truesdell et al., 1989; Capaccioni et al., 2016). Hence, any fractionation associated with evaporative $HCl_{(g)}$ loss may have a superimposed effect on the isotope signature of the lake water body. According to our experimental results, the sign of fractionation depends on the proportions of dissolved Cl-species in the lake water, so in theory, this may become either enriched or depleted in ^{37}Cl.

However, in a steady state situation with a continuous supply of hydrothermal fluid needed to sustain the volume of a warm evaporating lake (Pasternack and Varekamp, 1997), the loss of $HCl_{(g)}$ will be small relative to the amount of dissolved chlorine in the lake reservoir, making a major isotopic shift unlikely. The restricted $\delta^{37}Cl$ range between 0.0 and +1.2‰ found in acid crater lakes of volcanoes in subduction settings to date (Eggenkamp, 1994; Sharp et al., 2010; Rodríguez et al., 2016a) falls within the range between -3 and +3‰ reported for subduction-related volcanics (Barnes and Sharp, 2017; Liotta et al., 2017), suggesting that input signatures will generally be more important than evaporation effects in creating isotopic variations. Nevertheless, possible indications for an evaporation-induced Cl isotope shift come from the hyperacid crater lake of Poás volcano (Costa Rica) where long-term monitoring during almost three decades yielded $\delta^{37}Cl$ between +0.02±0.06‰ and +1.15±0.09‰, with some of the highest values recorded during an active period when the lake volume was reduced, temperature high and pH<0 (Rodríguez et al., 2016a). According to the fractionation mechanism inferred from our experiments, this strong acidity favoured the prevalence of HCl^0 as dissolved chlorine species, which should have promoted the predominant escape of the lighter Cl isotope as gaseous HCl. The evaporative $HCl_{(g)}$ loss is also reflected in increased Br/Cl ratios in the lake brine during the same time interval (Rodríguez et al., 2016a), in agreement with the lower volatilization rate of $HBr_{(g)}$ under extremely acid conditions seen in our experiments.

4.5. Implications for Mars

The widespread existence of evaporate material across the Martian surface indicates that fluid evaporation played an important role in the geologic past of the planet (Altheide et al., 2009). Hence, the results of our experiments are potentially significant for interpretations of $\delta^{37}Cl$ signatures of secondary Cl-bearing minerals considered to have formed through evaporative processes. The hypothesis of two Cl reservoirs on this planet is represented by a ^{37}Cl-depleted mantle from olivine-phyric shergottites ($\delta^{37}Cl$ = -3.8 to -2.0‰) and a ^{37}Cl-enriched crust from chassignites and nakhlites ($\delta^{37}Cl$ up to +8.6‰) (Sharp et al., 2016; Williams et al., 2016). The most negative values, found in olivine-phyric shergottites, have been taken to represent the primordial bulk composition of Mars, which the planet may have acquired during accretion, whereas the positive values, measured in other Martian meteorites, are suggestive of a ^{37}Cl enriched crust, possibly due to preferential loss of ^{35}Cl into space from the surface (Sharp et al. 2016; Williams et al., 2016). However, Bellucci et al. (2017) reported an average $\delta^{37}Cl$ content of −0.6‰ for apatites in shergottites with no textural, major element or halogen evidence for mixing with a surface reservoir. The authors concluded that the bulk Cl isotope compositions of Mars and Earth are not significantly different from each other and that the mixture of surface material with a crystallizing mafic or ultramafic magma is responsible for both negative (-5.6 to -0.2‰) and positive (+1.1 to +2.5‰) shifts in $\delta^{37}Cl$.

Tosca and McLennan (2006) have shown that, when starting from a solution that derived its cations from rock weathering, evaporation may develop a large spectrum of different brine compositions depending on the abundance and relative proportions of HCO_3^-, SO_4^{-2}, and Cl^- as principal anions. The authors proposed that saline mineral formation through evaporation on Mars, either proceeded in acid–sulphate dominated surficial environments or under conditions where acidity was buffered by basaltic weathering reactions and carbonates were produced. The evaporation path of the Kawah Ijen brine is more in line with the former option but is distinct in detail since the starting fluid is a hyperacid sulphate-chloride solution with an initial high load of cations due to rock dissolution. If halogen-rich brines with a similar hydrothermal origin existed on Mars (e.g., Schmidt et al., 2008; Yen et al., 2008), our findings indicate that evaporation-induced degassing of HCl will have either increased or decreased $\delta^{37}Cl$ in the residual solutions, since sign and magnitude of fractionation seem controlled by pH-dependent distribution of the Cl-species. Cases of ^{37}Cl enrichment may signal a very

strong acidity since a preferred escape of the lighter isotope presumably requires a prevalence of aqueous HCl^0 over Cl^-. In view of this mechanism, HCl degassing alone is inadequate as explanation for the elevated $\delta^{37}Cl$ signatures of nahklites, since the hydrothermal fluid inferred to have infiltrated the parent rock was CO_2 rich and had a circum-neutral pH (Bridges and Schwenzer, 2012; Filiberto et al., 2014). More likely, fractionation accompanying precipitation and removal of a Cl-bearing phase may have driven $\delta^{37}Cl$ to the positive values. Also, if the extremely light and highly variable $\delta^{37}Cl$ values (from -51±5‰ to -1±7‰) measured in sedimentary rocks and sand in Gale Crater by the SAM instrument on the Curiosity Rover (Farley et al., 2016) are correct, the Cl-hosting mineral(s) could not have been precipitated from an acidic brine that had undergone simple HCl evaporation. Although, according to our experiments, it is conceivable that HCl loss could drive the residual solution to lower $\delta^{37}Cl$, the fractionation factor would not be sufficient to reach the extreme negative values starting from a Martian mantle value, if Rayleigh-type fractionation is assumed. More likely, unusual low $^{37}Cl/^{35}Cl$ ratios are attributable to involvement of perchlorates, either as component in measured material or as its precursor (Farley et al., 2016; Bellucci et al., 2017). Our experiments also highlight the possibility that aqueous bromine and chlorine can become fractionated as a result of unequal evaporation rates of $HCl_{(g)}$ and $HBr_{(g)}$. This mechanism, together with precipitation of halogen-bearing minerals, could explain the variability of Br/Cl ratios and frequent Br-enrichments in soils of Gusev Crater and Meridiani Planum (e.g., Gellert et al., 2006; Marion et al., 2009).

The modelled progressive reduction of water activity in our experimental liquid can be used to estimate the theoretical freezing temperature of a residual Martian brine that experienced extensive evaporation (Chevrier and Altheide, 2008; Elsenousy et al., 2015):

$$T_E = \frac{1}{\frac{1}{T_0} - \frac{R\ ln a_{H_2O}}{\Delta H_f}} \tag{12}$$

$$\Delta H_f = 3.34768 + \frac{1.85714}{1 + exp\left(\frac{a_{H_2O} - 0.53822}{0.05031}\right)} + 1.855921 \cdot a_{H_2O} \tag{13}$$

Where T_E is the freezing temperature, R is the ideal gas constant, a_{H_2O} is the activity of water, T_0= 273.15 K; and ΔH_f is the enthalpy of fusion.

If similar hyperacid brines as that of Kawah Ijen would have been created on Mars (e.g., as a result of interaction of magmatic volatiles and ice, combined with intense water-rock interaction), the lowest a_{H_2O} value of 0.85 reached in our simulation predicts freezing temperatures down to 183 K (-90.15°C). This is close to the freezing point for the acids of Cl^- and SO_4^{2-} (Clark and Van Hart, 1981), which are among the strongest freezing point depressors. Taking the yearly average temperature of 240 K (-33.15°C) on Mars´ surface into account (Mellon et al., 2004), the stability of liquid water on the planet would thus be significantly enhanced by the existence of compositionally equivalent hyperacid brines. A final corollary is that the extreme chemistry of such evaporating brines, notably the combination of very low pH, low water activity and high salinity, has a negative effect on Martian habitability (Fox-Powell et al., 2016).

5. SUMMARY AND CONCLUSIONS

A 73-days long experiment on crater lake water from Kawah Ijen volcano (Indonesia) was carried out to study the chemical evolution of highly saline, hyperacid sulphate-chloride brine during extended evaporation, with special attention to chlorine isotope fractionation associated with the escape of gaseous HCl. Up to 58% evaporative water loss from the brine (starting pH ca. 0.1, TDS ca. 100 mg/kg) was accompanied by increasing contents of dissolved rock-forming elements, sulphur and halogens. Despite the high load and diversity of solutes, newly formed solid phases were restricted to Sr-bearing gypsum and possibly amorphous silica. The limited capability of producing evaporite minerals relative to that of seawater and other brine types apparently signals strongly enhanced metal solubilities due to complexation with abundantly available HSO_4^-, Cl^- and F^-.

Continuous loss of $HCl_{(g)}$ throughout the experiment permitted deriving quantitative insight into Cl-isotope fractionation between aqueous and gaseous chlorine. Monitoring the residual solution revealed a marked change in sign and magnitude of fractionation when evaporation proceeded. In the first three weeks of the experiment, the evaporating $HCl_{(g)}$ was isotopically heavier than the chlorine remaining in solution. Assuming Rayleigh-type behaviour, the calculated fractionation factor ($1000 \ln \alpha_{\mathrm{HCl_g - Cl_{diss.}}}$) was from $+1.55 \pm 0.49$‰ to $+3.37 \pm 1.10$‰, depending on the method for determining the Cl losses from the brine. In contrast, the evaporating $HCl_{(g)}$ became isotopically

lighter in the subsequent interval, with a corresponding fractionation factor between -5.67±0.17‰ and -3.97±0.08‰, more in line with existing experimental data (Sharp et al., 2010). The change in behaviour coincided with a transition from Cl^- to HCl^0 as the dominant chlorine species in the solution when pH had dropped below ca. -0.2. It is inferred that the distribution of dissolved Cl species exerts a strong control on sign and magnitude of Cl isotope fractionation during $HCl_{(g)}$ evaporation from an acid brine. Because evidence for $HBr_{(g)}$ loss is tenuous and the escape of $HCl_{(g)}$ is clearly more efficient, selective evaporation can also be an effective mechanism to fractionate Cl from Br and other solutes in acidic sulphate-chloride brines.

In most cases, surface evaporation of $HCl_{(g)}$ will have little effect on the Cl isotope compositions or Cl/Br ratios of sizable active volcanic lakes due to the large mass of dissolved chlorine compared to the evaporated fraction and the continuous supply of magmatic volatiles that usually mark these reservoirs. Detectible fractionation effects in hyperacid lakes may be limited to periods of enhanced evaporation and volume reduction.

The results of this work may provide new clues on the origin of Cl isotope signatures and Cl/Br variability in Martian soils and minerals. If evaporation of highly acidic fluids played a role, preferential loss of $HCl_{(g)}$ would yield a relative enrichment of Br and a shift in Cl-isotope composition either in positive or in negative direction, depending on the speciation of aqueous chlorine and thus on pH. It is conceivable that such effects are preserved in halogen-bearing salts and other solid residues of evaporation. Finally, the (former) presence of hyperacid sulphate-chloride brines as studied here would extend the stability of liquid water on the planet's surface to extremely low temperatures.

ACKNOWLEDGMENTS

All laboratory analyses were performed with the instrumental facilities of the Department of Earth Sciences, Utrecht University. We are grateful to Arnold van Dijk for carrying out the mass spectrometer measurements, and to Helen de Waard, Ton Zalm and Dineke van de Meent for help with experiments, ICP-OES and IC analyses, respectively. Our appreciation also goes to Helen King for expert support with Raman spectroscopy and SEM techniques, and to Sergei Matveev for the skilful EPMA work. The

manuscript benefited from the valuable comments of the reviewers. Funding for this research was provided by NWO (Netherlands Organization for Scientific Research), project ALW-GO-PL/10-03. H.G.M. Eggenkamp has received funding from the European Union's Horizon 2020 research and innovation programme as Individual Fellow under the Marie Skłodowska-Curie Actions (grant agreement N°702001, BRISOACTIONS). This is IPGP contribution 3884.

REFERENCES

Aiuppa A., Baker D. R. and Webster J. D. 2009. Halogens in volcanic systems. *Chem. Geol.* **263**, 1-18.

Altheide T., Chevrier V., Nicholson C. and Denson J., 2009. Experimental investigation of the stability and evaporation of sulfate and chloride brines on Mars. *EPSL* **282**, 69-78.

Azimi G. and Papangelakis V.G., 2011. Mechanism and kinetics of gypsum-anhydrite transformations in aqueous electrolyte solutions. *Hydrometallurgy* **108**, 122-129.

Azimi G., Papangelakis V.G., Dutrizac J.E., 2007. Modelling of calcium sulphate solubility in concentrated multi-component sulphate solutions. *Fluid Phase Equilib.* **260**, 300–315.

Barnes J.D. and Sharp Z.D., 2017. Chlorine isotope geochemistry. In: *Non-Traditional Stable Isotopes* (eds. F.Z. Teng, J. Watkins and N. Dauphas). Rev. Min. Geochem. **82**, 345-378.

Bell J., McSween H., Crisp J., Morris R., Murchie S., Bridges N., Johnson J., Britt D., Golombek M., Moore H., Ghosh A., Bishop J., Anderson R., Bruckner J., Economou T., Greenwood J., Gunnlaugsson H., Hargraves R., Hviid S., Knudsen J., Madsen M., Reid R., Rieder R. and Soderblom L., 2000. Mineralogic and compositional properties of Martian soil and dust: Results from Mars Pathfinder. *J Geophysical Res.* **105**, 1721-1755.

Bellucci J.J., Whitehouse M.J., John T., Nemchin A.A., Snape J.F., Bland P.A. and Benedix G.K., 2017. Halogen and Cl isotopic systematics in Martian phosphates: Implications for the Cl cycle and surface halogen reservoirs on Mars. *Earth Planet. Sci. Lett.* **458**, 192–202.

Brass G.W., 1980. Stability of brines on Mars. *Icarus* **42**, 20-28.

Bridges J.C. and Schwenzer S.P., 2012. The nakhlite hydrothermal brine on Mars. *Earth Planet. Sci. Lett.* **359–360**, 117–123.

Capaccioni B., Rouwet D. and Tassi F., 2016. HCl degassing from extremely acidic crater lakes: preliminary results from experimental determinations and implications for geochemical monitoring. In: *Geochemistry and Geophysics of Active Volcanic Lakes.* (eds. T. Ohba, B. Capaccioni and C. Caudron) Geological Society of London Special Publications, **437**, http://doi.org/10.1144/SP437.11.

Caudron C., Campion R., Rouwet D., Lecocq T., Capaccioni B., Syahbana D., Supergun, Purwanto B.H. and Bernard A., 2017. Stratification at the Earth's largest hyperacidic lake and its consequences. *Earth Planet. Sci. Lett*. **459**, 28-35.

Chevrier V.F. and Altheide T.S., 2008. Low temperature aqueous ferric sulfate solutions on the surface of Mars. *Geophys. Res. Lett* **35**, L22101, doi: 10.1029/2008GL035489.

Christenson B.W. and Wood C.P., 1993. Evolution of a vent-hosted system beneath Ruapehu Crater Lake, New Zealand. *Bull. Volcanol*. **55**, 547-565.

Clark B.C. and Van Hart D.C., 1981. The salts of Mars. *Icarus* **45**, 370-378.

Clark B.C., Morris R.V., McLennan S.M., Gellert R., Jolliff B., Knoll A.H., Squyres S.W., Lowenstein T.K., Ming D.W., Tosca N.J., Yen A., Christensen P.R., Gorevan S., Bruckner J., Calvin W., Dreibus G., Farrand W., Klingelhoefer G., Waenke H., Zipfel J., Bell J. F., Grotzinger J., McSween H.Y. and Rieder R., 2005. Chemistry and mineralogy of outcrops at Meridiani Planum. *Earth Planet. Sci. Lett*. **240**, 73-94.

Czarnacki M. and Halas S., 2012. Isotope fractionation in aqua-gas systems: Cl_2-HCl-Cl^-, Br_2-HBr-Br^- and H_2S-S^{2-}. *Isot. Environ. Health Stud.* **48**, 55-64.

Delmelle P. and Bernard A., 1994. Geochemistry, mineralogy and chemical modelig of the acid crater lake of Kawah-Ijen Volcano, Indonesia. *Geochim. Cosmochim. Acta* **58**, 2445-2460.

Delmelle P., Bernard A., Kusakabe M., Fischer T.P. and Takano B., 2000. Geochemistry of the magmatic-hydrothermal system of Kawah Ijen volcano, East Java, Indonesia. *J. Volcanol. Geotherm. Res.* **97**, 31-53.

Eggenkamp H.G.M., 1994. *The Geochemistry of chlorine isotopes.* PhD. thesis, Utrecht University, 150 p.

Elsenousy A., Hanley J. and Chevrier V.F., 2015. Effect of evaporation and freezing on the salt paragenesis and habitability of brines at the Phoenix landing site. *Earth Planet. Sci. Lett.* **421**, 39-46.

Farrah H.E., Lawrance G.A., Wanless E.J., 2004. Gypsum-anhydrite transformation in hot acidic manganese sulphate solution. A comparative kinetic study employing several analytical methods. *Hydrometallurgy* **75**, 91–98.

Farley K.A., Martin P., Archer Jr. P.D., Atreya S.K., Conrad P.G., Eigenbrode J.L., Fairén A.G., Franz H.B., Freissinet C., Glavin D.P., Mahaffy P.R., Malespín C., Ming D.W., Navarro-González R. and Sutter B., 2016. Light and variable $^{37}Cl/^{35}Cl$ ratios in rocks from Gale Crater, Mars: Possible signature of perchlorate. *Earth Planet. Sci. Lett*. **438,** 14-24.

Filiberto J., Treiman A.H., Giesting P.A., Goodrich C.A. and Gross J., 2014. High-temperature chlorine-rich fluid in the Martian crust: A precursor to habitability. *Earth Planet. Sci. Lett*. **401**, 110–115.

Foustoukus D. and Seyfried W.E. Jr, 2007. Fluid phase separation processes in hydrothermal systems. In: *Fluid-fluid interactions* (eds. A. Liebscher and C.A Heinrich), Rev. Min. Geochem. **65**, 213-233.

Fox-Powell M.G., Hallsworth J.E., Cousins C.R., Cockell C.S., 2016. Ionic strength is a barrier to the habitability of Mars. *Astrobiology* **16**, 427-442.

Freyer D., Voigt W., 2003. Invited review, crystallization and phase stability of $CaSO_4$ and $CaSO_4$-based salts. *Monatsh. Chem.* **134**, 693–719.

Gamazo P., Bea S.A., Saaltink M.W., Carrera J. and Ayora C., 2011. Modeling the interaction between evaporation and chemical composition in a natural saline system. *J. Hydrol.* **401**, 154-164.

Gellert R., Rieder R., Anderson R., Bruckner J., Clark B., Dreibus G., Economou T., Klingelhofer G., Lugmair G., Ming D., Squyres S., d'Uston C., Wanke H., Yen A. and Zipfel J., 2004. Chemistry of rocks and soils in Gusev crater from the Alpha Particle X-ray Spectrometer. *Science* **305**, 829-832.

Gellert R., Rieder R., Bruckner J., Clark B., Dreibus G., Klingelhofer G., Lugmair G., Ming D., Wanke H., Yen A., Zipfel J. and Squyres S., 2006. Alpha particle X-ray spectrometer (APXS): Results from Gusev crater and calibration report. *J. Geophys. Res.* **111**, E02S05.

Giggenbach W. F., 1975. Variations in the carbon, sulfur and chlorine contents of volcanic gas discharges from White Island, New Zealand. *Bull. Volcanol.* **39**, 15-27.

Giggenbach W.F., 1987. Redox processes governing the chemistry of fumarolic gas discharges from White Island, New Zealand. *Appl. Geochem.* **2**, 143-161.

Gorrepati E.A., Wongthahan P., Raha S., and Fogler H.S., 2010. Silica precipitation in acid solutions: mechanism, pH effect and salt effect. Langmuir 26, 10467-10474.

Gunnarsson I. and Arnórsson S., 2000. Amorphous silica solubility and the thermodynamic properties of $H_4SiO^0_4$ in the range of 0° to 350°C at P_{sat}. *Geochim. Cosmochim. Acta* **64**, 2295-2307.

Hardie L.A., 1967. The gypsum–anhydrite equilibrium at one atmosphere. *Am. Mineral.* **52**, 171–200.

Haskin L., Wang A., Jolliff B., McSween H., Clark B., Des Marais D., McLennan S., Tosca N., Hurowitz J., Farmer J., Yen A., Squyres S., Arvidson R., Klingelhofer G., Schroder C., de Souza P., Ming D., Gellert R., Zipfel J., Bruckner J., Bell J., Herkenhoff K., Christensen P.,

Ruff S., Blaney D., Gorevan S., Cabrol N., Crumpler L., Grant J. and Soderblom L., 2005. Water alteration of rocks and soils on Mars at the Spirit rover site in Gusev crater. *Nature* **436**, 66-69.

Ichikuni M. and Musha S., 1978. Partition of strontium between gypsum and solution. *Chem. Geol.* **21**, 359-363.

Innorta G., Rabbi E. and L. Tomadin, 1980. The gypsum-anhydrite equilibrium by solubility measurements. Geochim. Cosmochim. Acta 44, 1931–1936.

Johnson K.S. and Pytkowicz R.M., 1978. Ion association of the Cl^- with H^+, Na^+, K^+, Ca^{2+} and Mg^{2+} in aqueous solutions at 25°C. *Am. J. Sci.* **278,** 1428-1447.

Kaufmann R.S., 1984. *Chlorine in groundwater: stable isotope distribution.* PhD. thesis, University of Arizona, 137 p.

Kempter K.A. and Rowe G.L., 2000. Leakage of active crater lake brine through the north flank at Rincón de la Vieja volcano, northwest Costa Rica, and implications for crater collapse. *J. Volcanol. Geot. Res.* **97**, 143-159.

Knauth L.P. and Burt D.M., 2002. Eutectic Brines on Mars: Origin and Possible Relation to Young Seepage Features. *Icarus* **158**, 267-271.

Kushnir J., 1980. The coprecipitation of strontium, magnesium, sodium, potassium and chloride ions with gypsum. An experimental study. *Geochim. Cosmochim. Acta* **44**, 1471-1482.

Li Z., Demopoulos G.P., 2006. Model-based construction of calcium sulphate phase transition diagrams in the HCl–$CaCl_2$–H_2O system between 0 and 100 °C. *Ind. Eng. Chem. Res.* **45**, 4517–4524.

Li L., Boniface M., Aubaud C., Crispi O., Déssert C. and Agrinier P., 2015. Chlorine isotopes of thermal springs in arc volcanoes for tracing shallow magmatic activity. *Earth Planet. Sci. Lett*. **413**, 101 –110.

Liebscher A., Lüders V., Heinrich C. and Schettler, 2006. Br/Cl signature of hydrothermal fluids: liquid-vapor of bromine revised. *Geofluids* **6,** 113-121.

Liotta M., Rizzo A.L., Barnes J.D., D'Auria L., Martelli, M., Bobrowski, N. Wittmer J., 2017. Chlorine isotope composition of volcanic rocks and gases at Stromboli volcano (Aeolian Islands, Italy): Inferences on magmatic degassing prior to 2014 eruption. *J. Volcanol. Geot. Res.* **336**, 168-178.

Marcus, Y., 1979. Ionic dissociation of aqueous hydrobromic acid. Part 1.-Estimate from vapour pressure and activity coefficient data. J. Chem. Soc., Faraday Trans. 1, 75, 1715-1727.

Marshall W.L. and Warakomski J.M., 1980. Amorphous silica solubilities II. Effect of aqueous salt solutions at 25°C. *Geochim. Cosmochim. Acta* **44**, 915-924.

Mellon M.T., Feldman W.C. and Prettyman T.H., 2004. The presence and stability of ground ice in the southern hemisphere of Mars. *Icarus* **169**, 324-340.

Nordstrom D., Alpers C., Ptacek C. and Blowes D., 2000. Negative pH and extremely acidic mine waters from Iron Mountain, California. *Environ. Sci. Technol.* **34**, 254-258.

Ossorio M., van Driessche A.E.S., Pérez P., García-Ruiz J.M., 2014. The gypsum-anhydrite paradox revised. *Chem. Geol. 386*, 16-21.

Ostroff A.G., 1964. Conversion of gypsum to anhydrite in aqueous salt solutions. *Geochim. Cosmochim. Acta* **28**, 1363–1372.

Parkhurst D.L. and Appelo C.A.J., 1999. User's guide to PHREEQC (Version 2), A computer program for speciation, batch-reaction, one-dimensional transport, and inverse geochemical calculations. USGS Report 99-4259, 312 p.

Pasternack G.B. and Varekamp J.C., 1997. Volcanic lake systematics 1. Physical constraints. *Bull. Volcanol.* **58**, 528-538.

Pitzer K.S. and Mayorga G., 1973. Thermodynamics of electrolytes II. Activity and osmotic coefficients for strong electrolytes with one or both ions univalent. *J. Phys. Chem.* **77**, 2300-2308.

Posnjak E., 1938. The system, $CaSO_4$–H_2O. *Am. J. Sci.* **35A**, 247–272.

Posnjak E., 1940. Deposition of calcium sulphate from seawater. *Am. J. Sci.* **238**, 559–568.

Rodríguez A. and van Bergen M.J., 2015. Volcanic hydrothermal systems as potential analogues of Martian sulphate-rich terrains. Nederlands Journal of Geosciences http://dx.doi.org/10.1017/njg.2015.12.

Rodríguez A. and van Bergen M.J., 2017. Superficial alteration mineralogy in active volcanic systems: An example of Poás volcano, Costa Rica. *J. Volcanol. Geotherm. Res.* https://doi.org/10.1016/j.jvolgeores.2017.04.006.

Rodríguez A., Eggenkamp H.G.M., Martínez-Cruz M. and van Bergen M.J., 2016a. Chlorine isotope and Cl–Br fractionation in fluids of Poás volcano (Costa Rica): Insight into an active volcanic–hydrothermal system. *J. Volcanol. Geotherm. Res*. **325**, 70-85.

Rodríguez A., Varekamp J.C., van Bergen M.J., Kading T.J., Oonk P.B., Gammons C.H. and Gilmore M., 2016b. Acid rivers and lakes at Caviahue-Copahue volcano as potential terrestrial analogues for aqueous paleo-environments on Mars. In: *Copahue volcano.* (eds.) F. Tassi, O. Vaselli and A. Caselli. Springer, pp. 141-172.

Rouwet D. and Ohba T., 2015. Isotope fractionation and HCl partitioning during evaporative degassing from active lakes. In: *Volcanic Lakes.* (eds. D. Rouwet, BW Christenson, F. Tassi and J. Vandemeulebrouck). Springer, pp. 179-200.

Rouwet D., Tassi F., Mora-Amador R., Sandri L. and Chiarini V., 2014. Past, present and future of volcanic lake monitoring. *J. Volcanol. Geotherm. Res.* **272**, 78-97.

Rouwet D., Mora-Amador R., Ramírez-Umaña C.J., González G. and Inguaggiato S., 2016. Dynamic fluid recycling at Laguna Caliente (Poás, Costa Rica) before and during the 2006–ongoing phreatic eruption cycle (2005–10). In: *Geochemistry and Geophysics of Active Volcanic Lakes.* (eds. T. Ohba, B. Capaccioni and C. Caudron) Geological Society of London Special Publications, **437**, http://doi.org/10.1144/SP437.11.

Rowe G.L., Brantley S.L., Fernández M., Fernández J.F., Borgia A. and Barquero J., 1992. Fluid-volcano interaction in an active stratovolcano: the crater lake system of Poás volcano, Costa Rica. *J. Volcanol. Geotherm. Res.* **49**, 23-51.

Schauble E.A., Rossman G.R. and Taylor Jr, H.P., 2003. Theoretical estimates of equilibrium chlorine-isotope fractionations. *Geochim. Cosmochim. Acta* **67**, 3267-3281.

Seo J.H. and Zajacz Z., 2016. Fractionation of Cl/Br during fluid phase separation in magmatic-hydrothermal fluids. *Geochim. Cosmochim. Acta* **183**, 125–137.

Sharp Z.D., Barnes J.D., Fischer T. P. and Halick M., 2010. An experimental determination of chlorine isotope fractionation in acid systems and applications to volcanic fumaroles. *Geochim. Cosmochim. Acta* **74**, 264-273.

Sharp Z.D., Williams J., Shearer C., Agee C. and McKeegan K., 2016. The chlorine isotope composition of Martian meteorites 2. Implications for the early solar system and the formation of Mars. *Meteoritics & Planetary Science* **51**, 2111-2126.

Schmidt M.E., Ruff S.W., McCoy T.J., Farrand W.H., Johnson J.R., Gellert R., Ming D.W., Morris R.V., Cabrol N., Lewis K.W. and Schroeder C., 2008. Hydrothermal origin of halogens at Home Plate, Gusev Crater. *J. Geophys. Res.* **113**, E06S12.

Toner J.D., Catling D.C. and Light B., 2015. Modeling salt precipitation from brines on Mars: Evaporation versus freezing origin for soil salts. *Icarus* **250**, 451-461.

Tosca N.J. and McLennan S.M., 2006. Chemical divides and evaporite assemblages on Mars. *Earth Planet. Sci. Lett.* **241**, 21-31.

Tosca N.J. and McLennan S.M., 2009. Experimental constraints on the evaporation of partially oxidized acid-sulfate waters at the Martian surface. *Geochim. Cosmochim. Acta* 73, 1205-1222.

Truesdell A.H., Haizlip J.R., Ármannsson H. and D'Amore F., 1989. Origin and transport of chloride in superheated geothermal steam. *Geothermics* **18**, 295-304.

Urey H.C. and Greiff L.J., 1935. Isotopic exchange equilibria. *J. Amer. Chem. Soc.* **54**, 3211-327.

Van Hinsberg V., Berlo K., van Bergen M. and Williams-Jones A., 2010. Extreme alteration by hyperacidic brines at Kawah Ijen volcano, East Java, Indonesia I. Textural and mineralogical imprint. *J. Volcanol. Geotherm. Res*. **198**, 253-263.

Varekamp J.C., Pasternack G.B. and Rowe G.L., 2000. Volcanic lake systematics II. Chemical constraints. *J. Volcanol. Geotherm. Res.* **97**, 161-179.Williams J.T., Shearer C.K., Sharp

Z.D., Burger P.V., McCubbin F.M., Santos A.R., Agee C.B. and McKeegan K.D., 2016. The chlorine isotopic composition of Martian meteorites 1: Chlorine isotope composition of Martian mantle and crustal reservoirs and their interactions. *Meteoritics & Planetary Science*, doi: 10.1111/maps.12647.

Von Damm K.L., Lilley M.D., Shanks W.C. III, Brockington M., Bray A.M., O'Grady K.M., Olson E., Graham A., Proskurowski G., and the SouEPR Science Party, 2003. Extraordinary phase separation and segregation in vent fluids from the southern East Pacific Rise. *Earth Planet. Sci. Lett*. **206**, 365–378.

Williams J.T., Shearer C.K., Sharp Z.D., Burger P.V., McCubbin F.M., Santos A.R., Agee C.B. and McKeegan, 2016. The chlorine isotopic composition of Martian meteorites 1: Chlorine isotope composition of Martian mantle and crustal reservoirs and their interactions. *Meteoritics & Planetary Science* **51**, 2092–2110.

Yen A.S., Morris R.V., Clark B.C., Gellert R., Knudson A.T., Squyres S., Mittlefehldt D.W, Ming D.W., Arvidson R., McCoy T., Schmidt M., Hurowitz J., Li R.9 and Johnson J.R., 2008. Hydrothermal processes at Gusev Crater: An evaluation of Paso Robles class soils. *J. Geophys. Res.* **113**, E06S10, doi: 10.1029/2007JE002978.

Zolotov M.Y. and Mironenko M.V., 2007. Timing of acid weathering on Mars: A kinetic-thermodynamic assessment. *J. Geophys. Res.* **112**, E07006.

FIGURE CAPTIONS

Figure 1. Experimental setup. Twenty-six plastic Greiner® tubes, each containing approximately 50 ml of brine, were partially submerged in a water bath at 60°C. The solutions were allowed to evaporate in air. Sampling was performed after a pre-set time interval when two tubes were removed and processed separately for analysis.

Figure 2. Time series of (a) evaporation loss (wt. %), (b) evaporation rate (g/h/dm^2) and (c) pH recorded during the experiment on the Kawah Ijen hyperacid brine. The error bars are smaller than the size of the symbols.

Figure 3. Element/Mg molar ratios recorded in the course of progressive evaporation for: (a) Cl, S_T; (b) F, 10xBr, B; (c) Ca, Sr; (d) Al, Si; (e) Na, Fe; (f) K, Ti. Horizontal trends point to conservative behaviour of most elements, whereas declining ratios indicate loss of Cl, Ca, Sr and Si through separation of gaseous (HCl) and solid (gypsum and possibly amorphous silica) phases. Note that the Y-axis scales are variable.

Figure 4. Time series trends for (a) fugacities of selected gaseous compounds and (b) saturation indices of selected minerals, calculated for the evaporating brine. Similar graphs for halides and sulphates with lower SI values are given in the Supplementary Electronic Annex EA-1.

Figure 5. (a) Raman spectra of gypsum precipitated in the course of the experiment. Reference spectra for anhydrite (R040012) and gypsum (R040029) are from the RRUFF database (www.rruff.info). (b) SEM image of gypsum crystals.

Figure 6. Time series of calculated activities (PHREEQC) for the main aqueous species of S(VI), Cl and Br in the residual evaporating brine. Similar graphs for metal-bearing species are given in the Supplementary Electronic Annex EA-2.

Figure 7. Evolution of $\delta^{37}Cl$ in the residual hyperacid brine in the course of progressive evaporation at T=60°C.

Figure 8. Factors for chlorine isotope fractionation between $HCl_{(g)}$ and $Cl_{diss.}$ ($\alpha_{HCl_{(g)}-Cl_{diss.}}$), assuming Rayleigh distillation. Mass-losses of Cl (*F* values) based on: (a) Cl concentrations and water losses, (b) Cl/B ratios, (c) Cl/Fe ratios, and (d) Cl/Mg ratios. Note the significant change in α value after approximately 500 hours of evaporation.

Figure 9. Measured $\delta^{37}Cl$ for dissolved Cl ($Cl_{diss,}$) and calculated $\delta^{37}Cl$ for gaseous Cl ($HCl_{(g)}$), based on (a) Cl mass loss, (b) Cl/B ratios, (c) Cl/Fe ratios, and (d) Cl/Mg ratios. Note the significant change in $\delta^{37}Cl$ after approximately 500 hours of evaporation.

Figure 10. Predicted amounts of secondary phases formed during progressive evaporation, based on PHREEQC simulation (T=60°C), as a function of (a) H_2O loss (wt. %) and (b) water activity (a_{H_2O}).

Figure 11. Activities of the main species of S(VI), Cl and Br according to simulated evaporation (PHREEQC) of the hyperacid brine at T=60°C. Note that curves for the activities of HCl^0 and Cl^- cross at high degrees of water loss. Similar graphs for activities of the main metal species are given in Supplementary Electronic Annex EA-5.

Figure 12. Br/Cl and S_T/Cl molar ratios recorded throughout the evaporation experiment. Increasing trends are consistent with loss of gaseous HCl.

Figure 13. Calculated distributions of dissolved Cl species in the course of the evaporation experiment on the hyperacid brine, expressed as percentage of the total Cl molality. Note that after 500 hours HCl^0 becomes more abundant than Cl^-.

TABLE CAPTIONS

Table 1. Recorded data for mass loss, pH, conductivity and evaporation rate during experimental evaporation of the hyperacid Kawah Ijen brine.

Table 2. Compositional changes in the hyperacid Kawah Ijen brine during experimental evaporation.

Table 3. Chlorine isotope evolution during experimental evaporation of the hyperacid Kawah Ijen brine, inferred from mass loss of the solution, $\delta^{37}Cl$ of dissolved Cl and inferred $HCl_{(g)}$ loss. Calculations of *F* values (fractions of Cl remaining in solution) based on differences between measured and calculated Cl concentrations, combined with water-vapour losses (see Table 1). $\delta^{37}Cl_{HCl_{(g)}}$ values obtained from calculated fractionation factors, assuming Rayleigh fractionation (see Figs. 8 and 9). The reported $1000\ln\alpha_{HCl_{(g)}-Cl_{diss.}}$ (‰) values assume a stepwise change in fractionation behaviour and are valid for the 0-500 hours and 500-1750 hours interval, respectively.

Table 4. Summary of chlorine isotope fractionation factors obtained from the evaporation experiments at T=60°C, based on Rayleigh fractionation and different approaches for calculating *F* factors (see Figs. 8 and 9, Table 3 and EA-3).

SUPPLEMENTARY ELECTRONIC ANNEX CAPTIONS

EA-1. Saturation indices of (a) halides, (b) Fe^{2+}-sulphates and (c) Mg-sulphates during the evaporation experiment.

EA-2. Time series of calculated activities (PHREEQC) of the main aqueous species of (a) Al, (b) Fe(II), (d) Fe(III), (e) Mg, (f) Ca, (g) K, (h) Na and (i) Sr. Note that the Y-axis scales are variable.

EA-3. Same as Table 3 but with *F* values calculated from Cl/B ratios assuming that B is perfectly conservative. The reported $1000\ln\alpha_{\mathrm{HCl_{(g)}-Cl_{diss.}}}(‰)$ values assume a stepwise change in fractionation behaviour and are valid for the 0-500 hours and 500-1750 hours interval, respectively. Additionally, *F* values are calculated from Cl/Fe and Cl/Mg ratios assuming that both Fe and Mg are conservative.

EA-4. Calculated changes in the saturation indices (PHREEQC) of: (a) hydrous iron (II) sulphates, (b) hydrous magnesium sulphates and (c) halides during progressive evaporation of the hyperacid brine at T=60°C.

EA-5. Activities of the main species of (a) Al, (b) Fe(II), (b) Fe(III), (d) Mg, (d) Ca, (f) K, (g) Na and (h) Sr according to simulated evaporation (PHREEQC) of the hyperacid brine at T=60°C. Note that the Y-axis scales are variable.

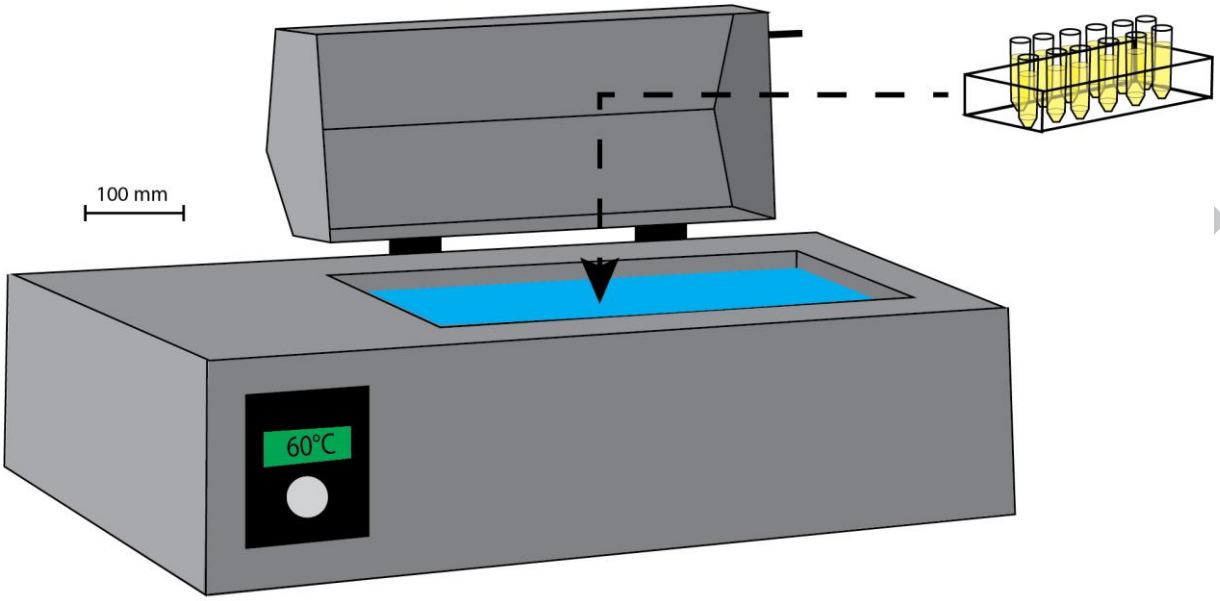

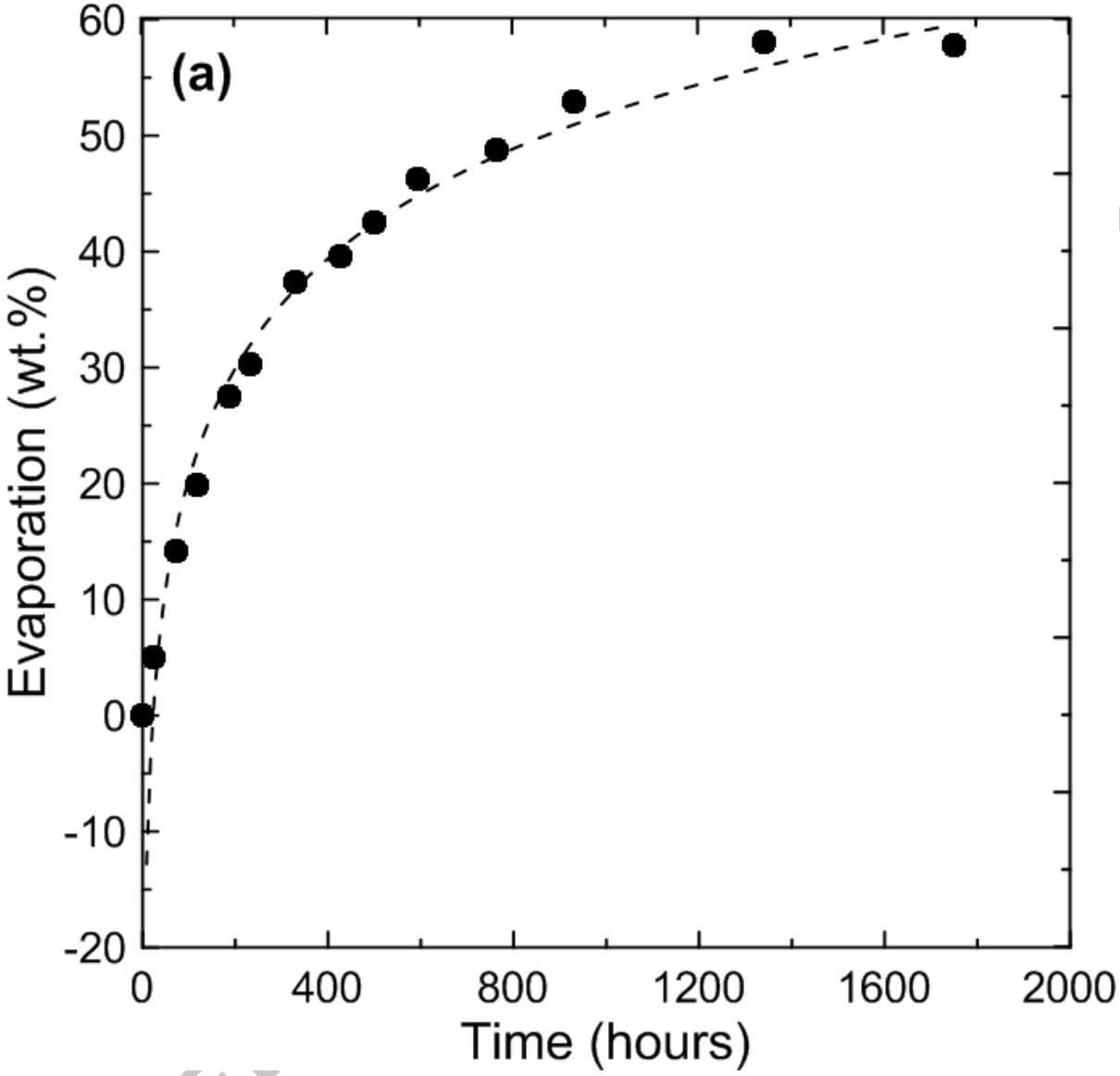
(a)
Evaporation (wt.%)
Time (hours)
60
50
40
30
20
10
0
-10
-20
0
400
800
1200
1600
2000

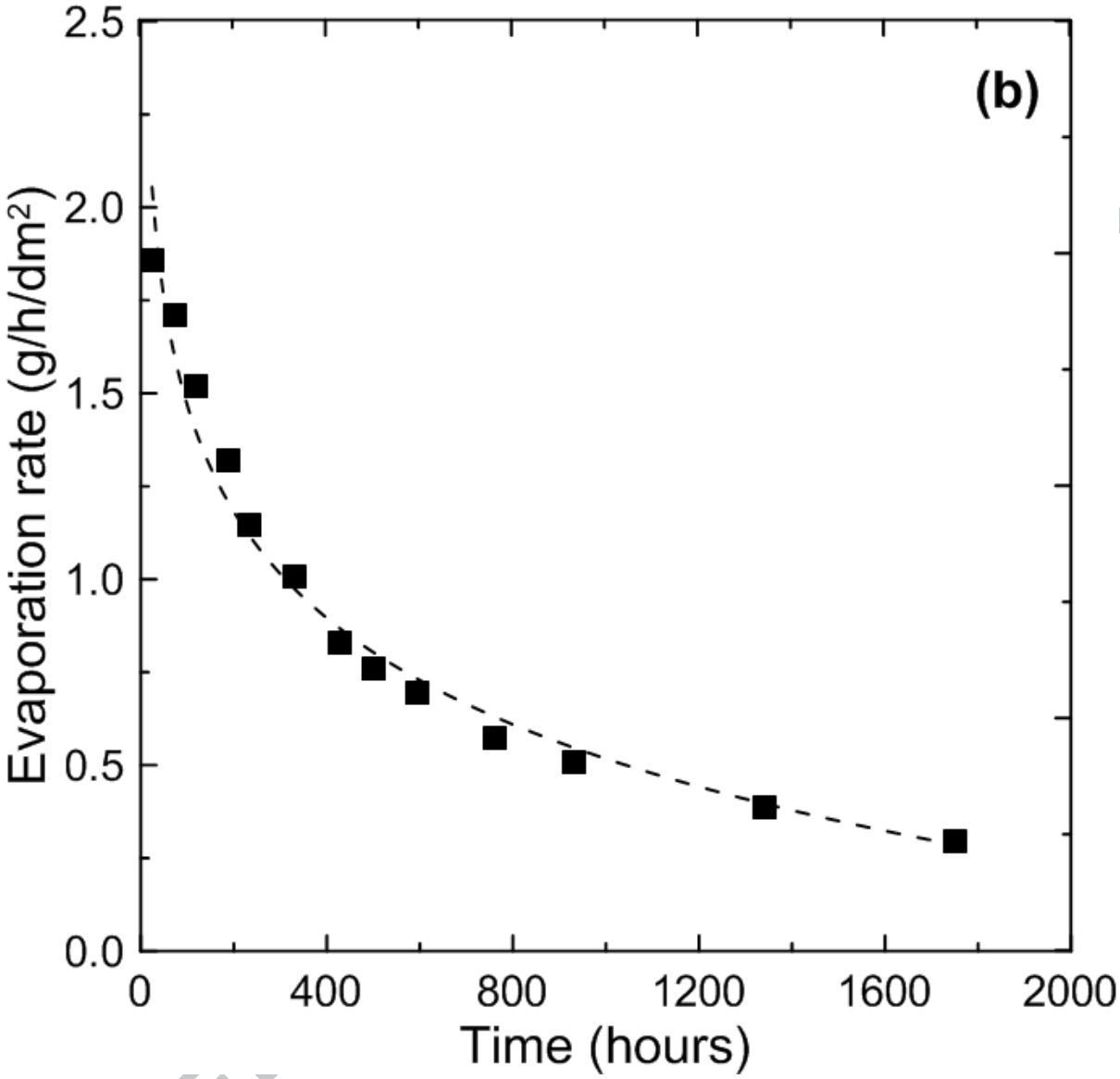
(b)
Evaporation rate (g/h/dm²)
Time (hours)
0.0
0.5
1.0
1.5
2.0
2.5
0
400
800
1200
1600
2000

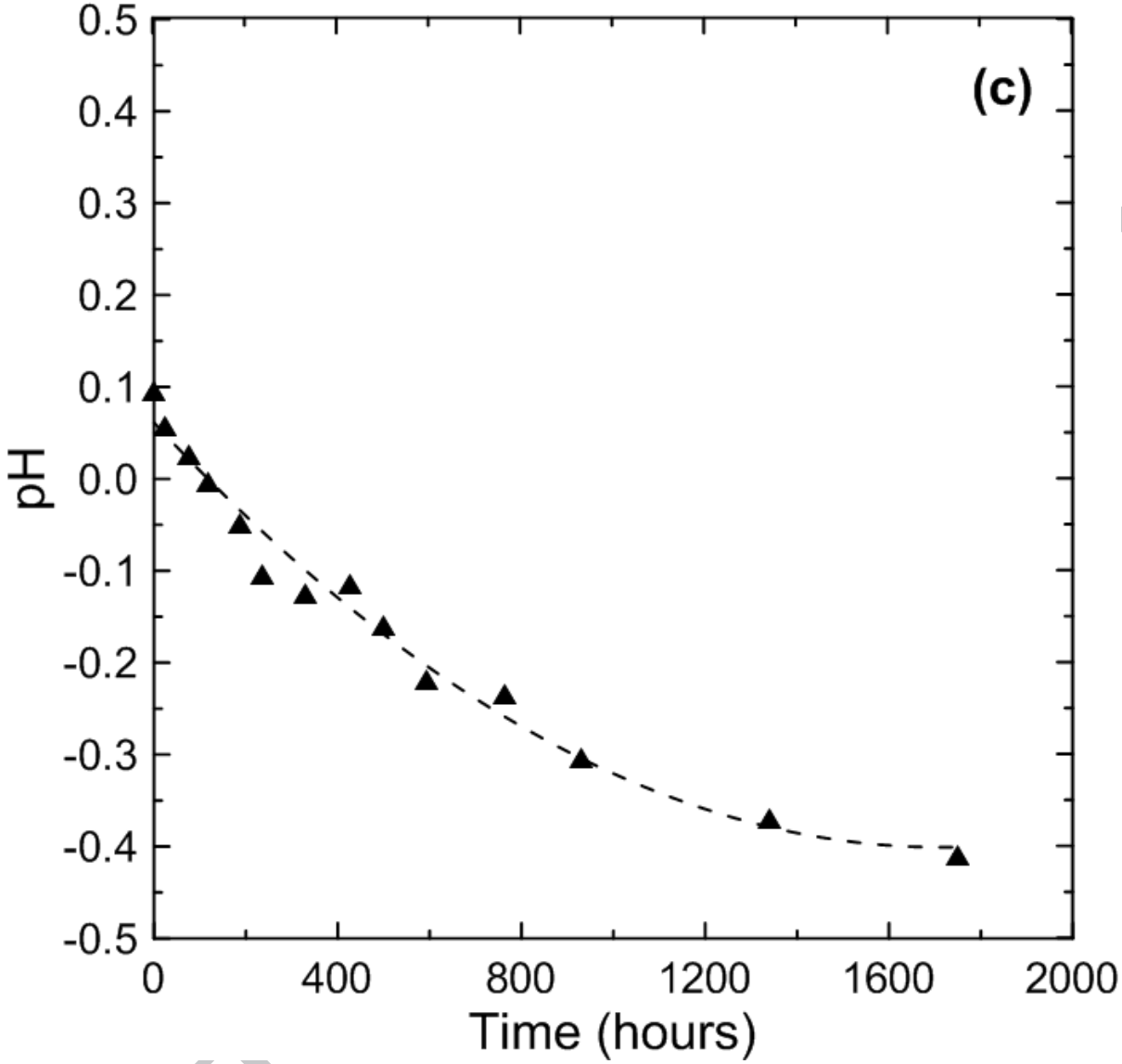
(c)
pH
Time (hours)
0.5
0.4
0.3
0.2
0.1
0.0
-0.1
-0.2
-0.3
-0.4
-0.5
0
400
800
1200
1600
2000

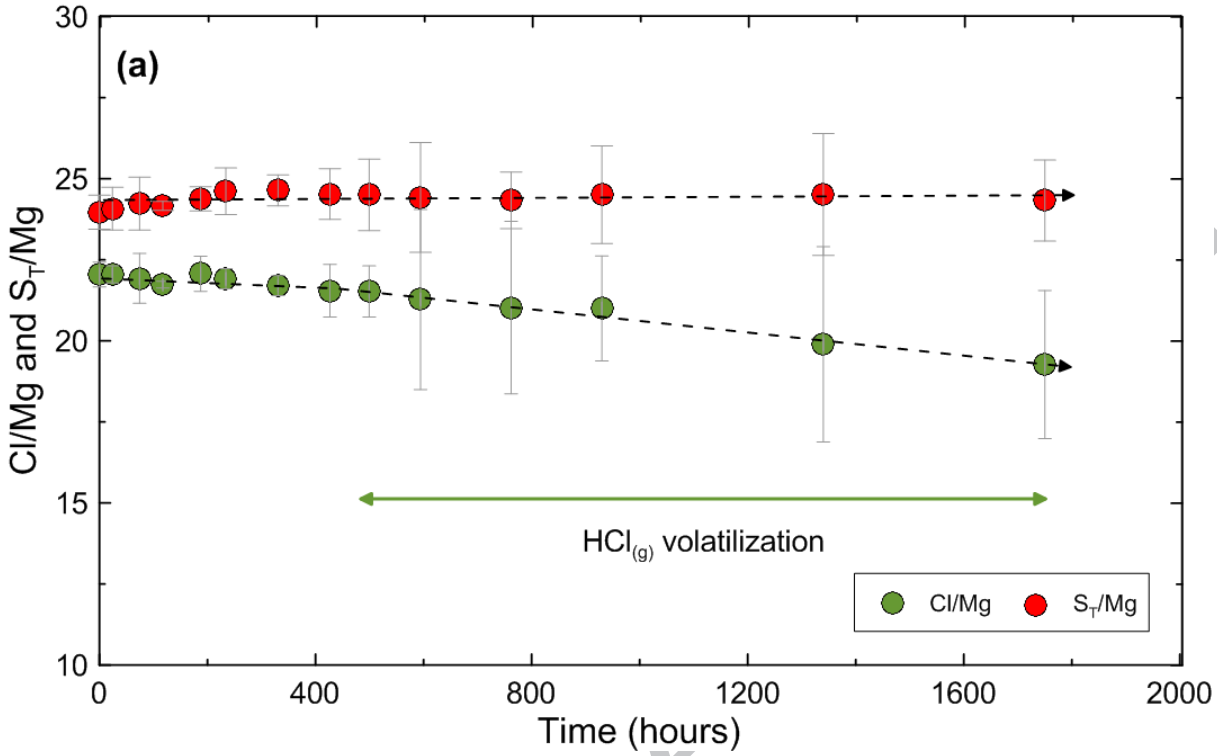

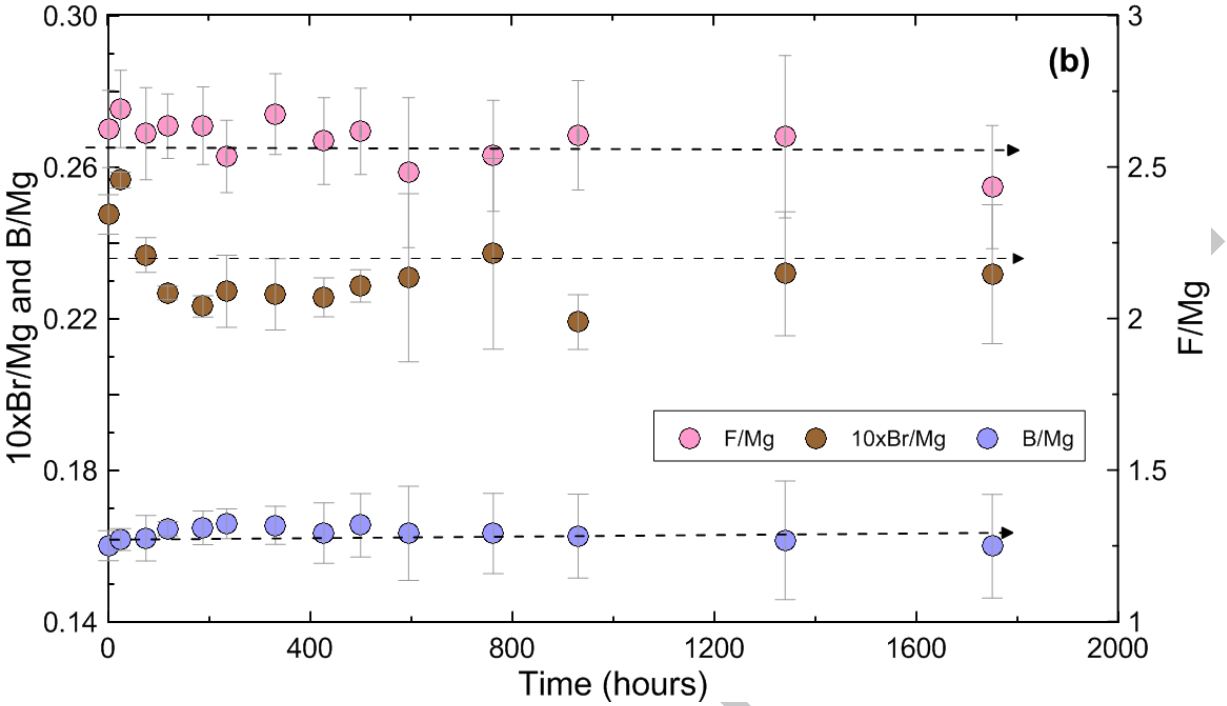

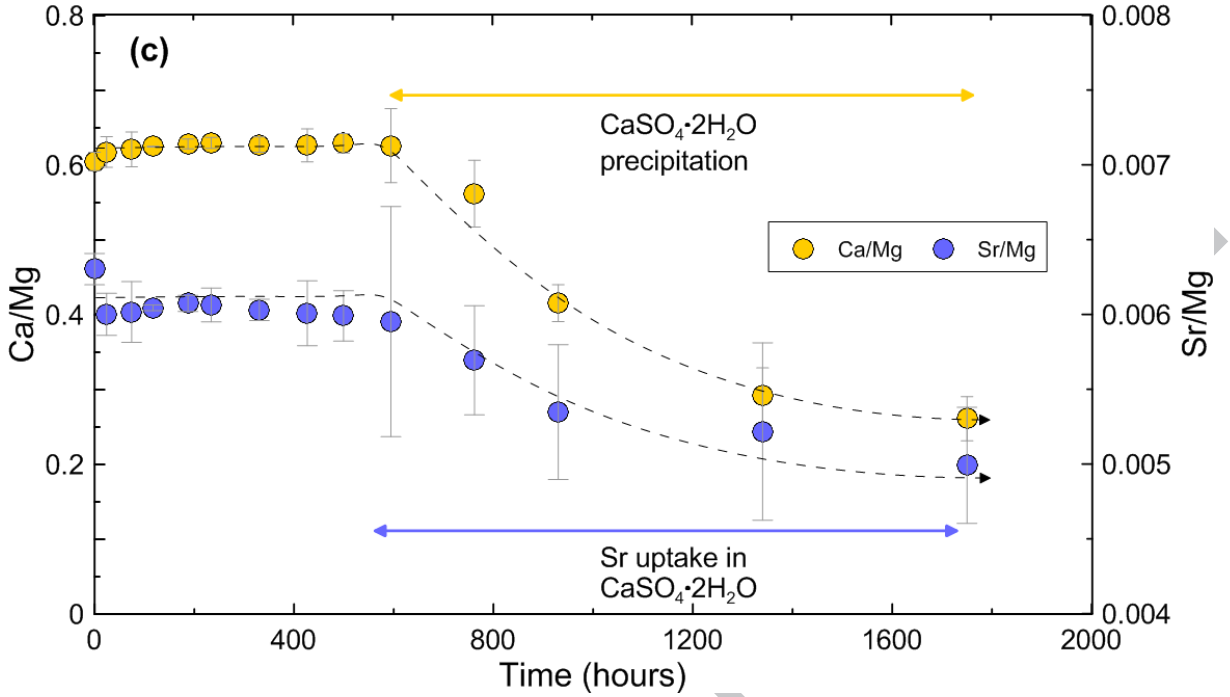

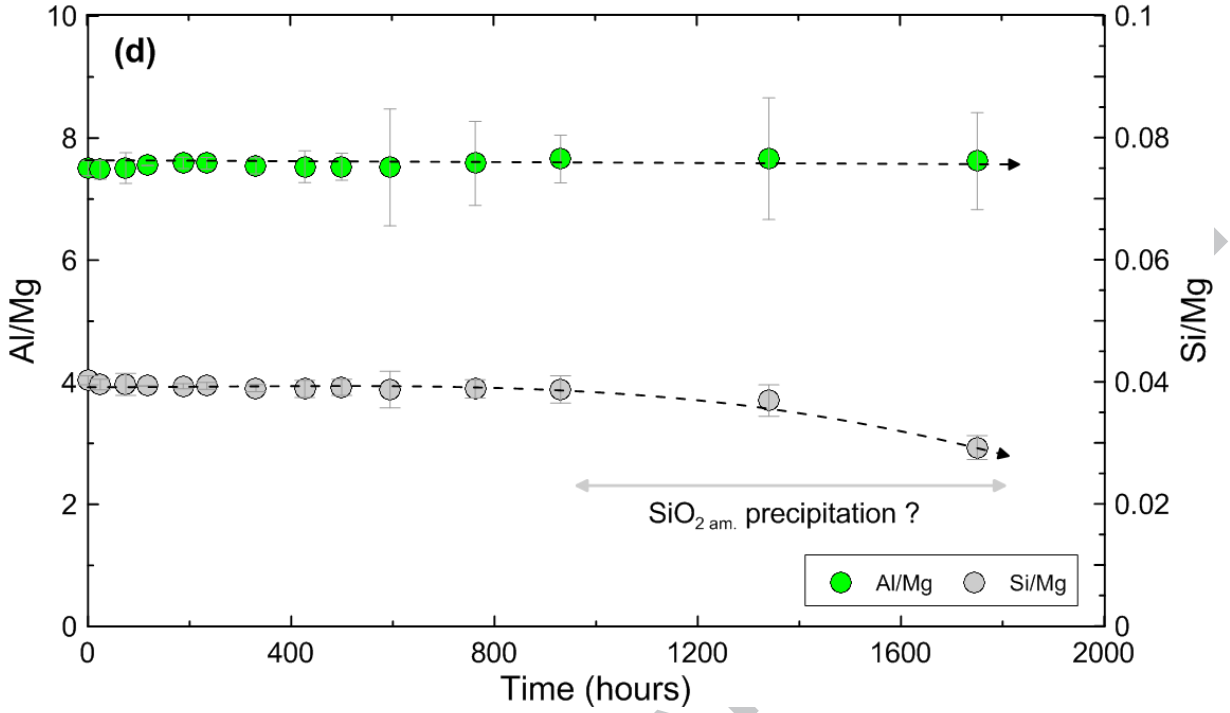

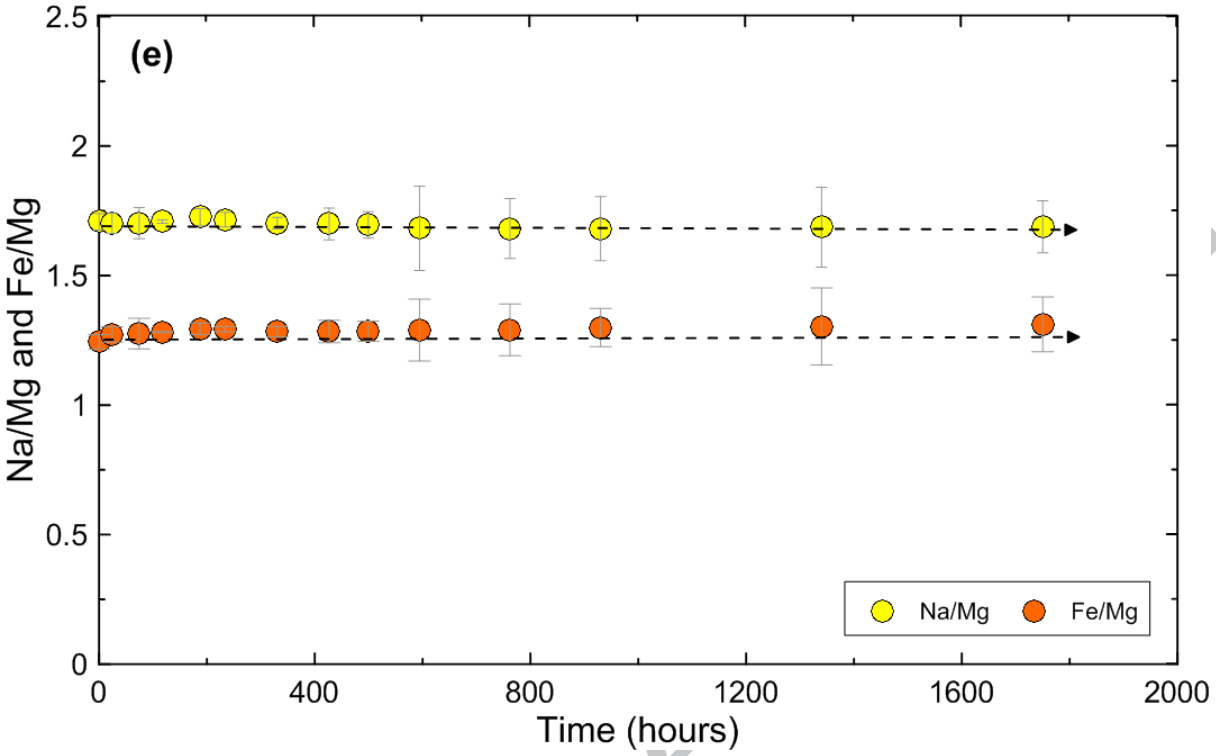

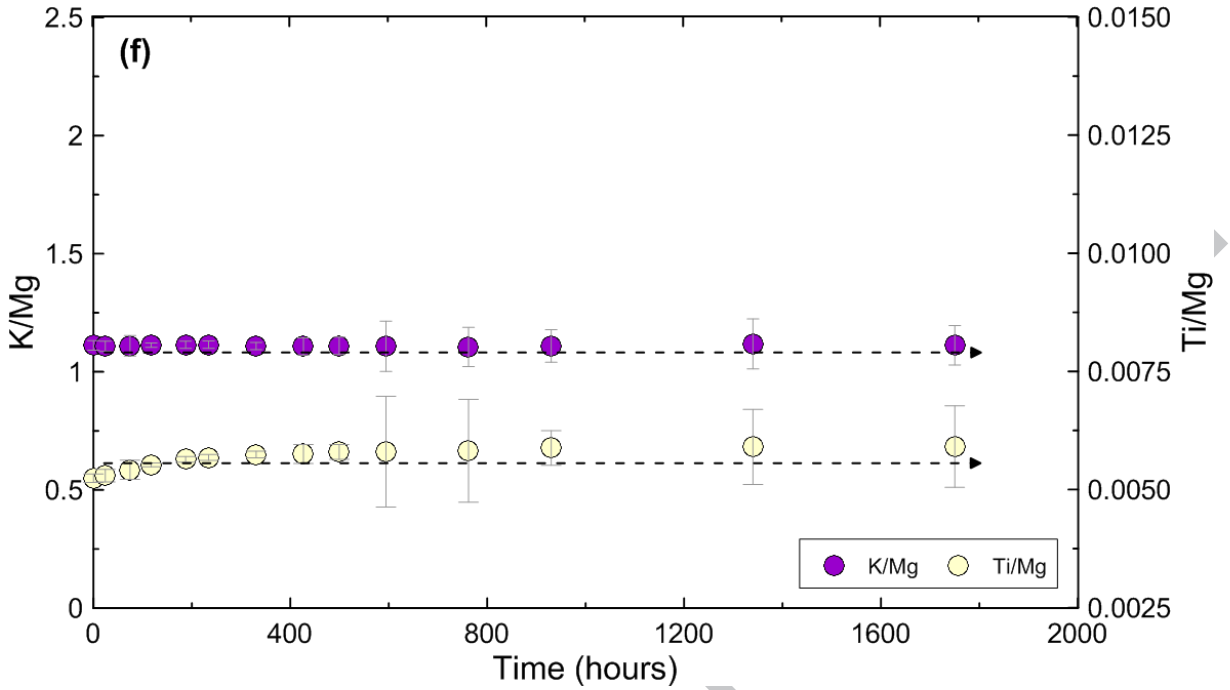

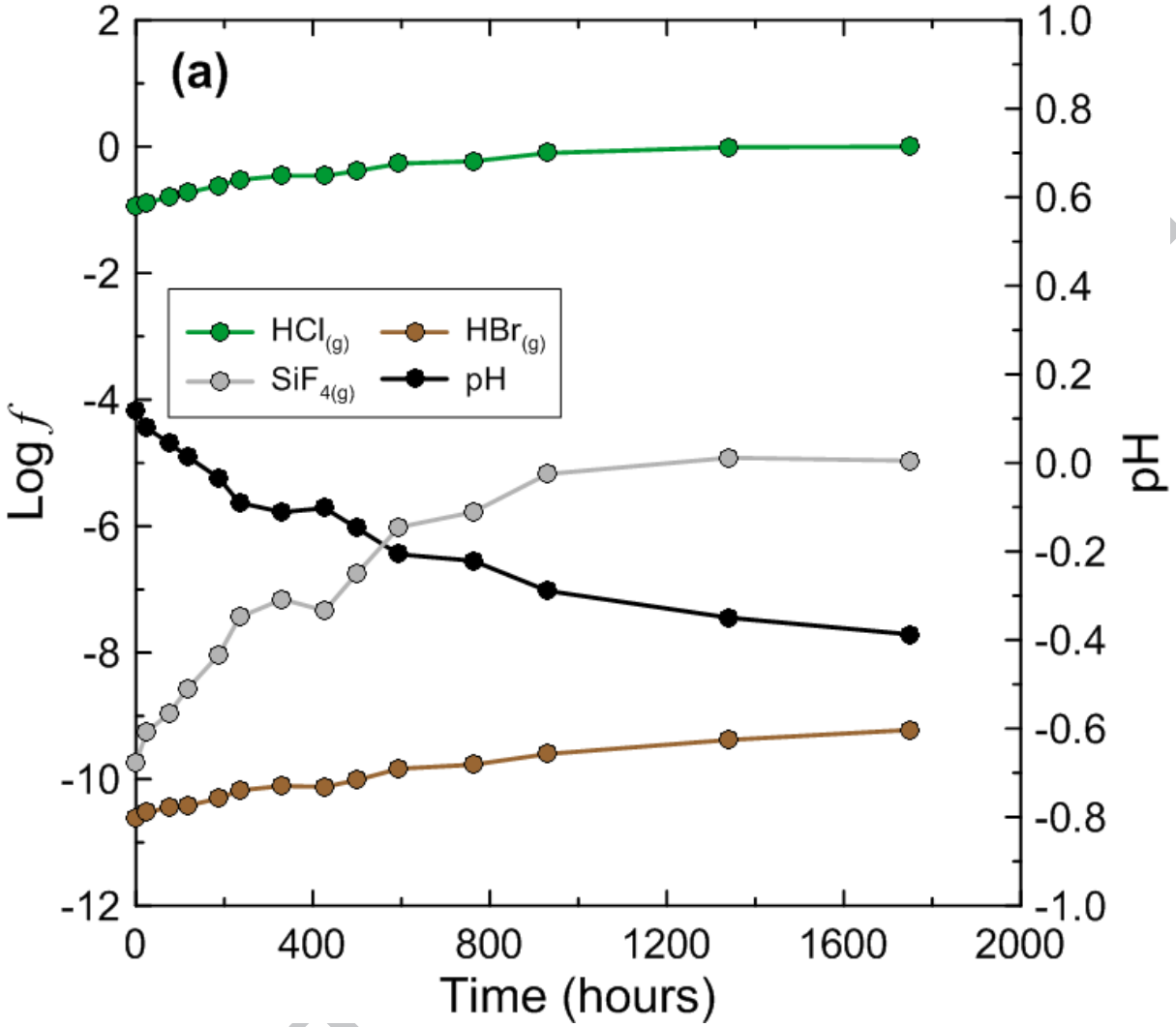

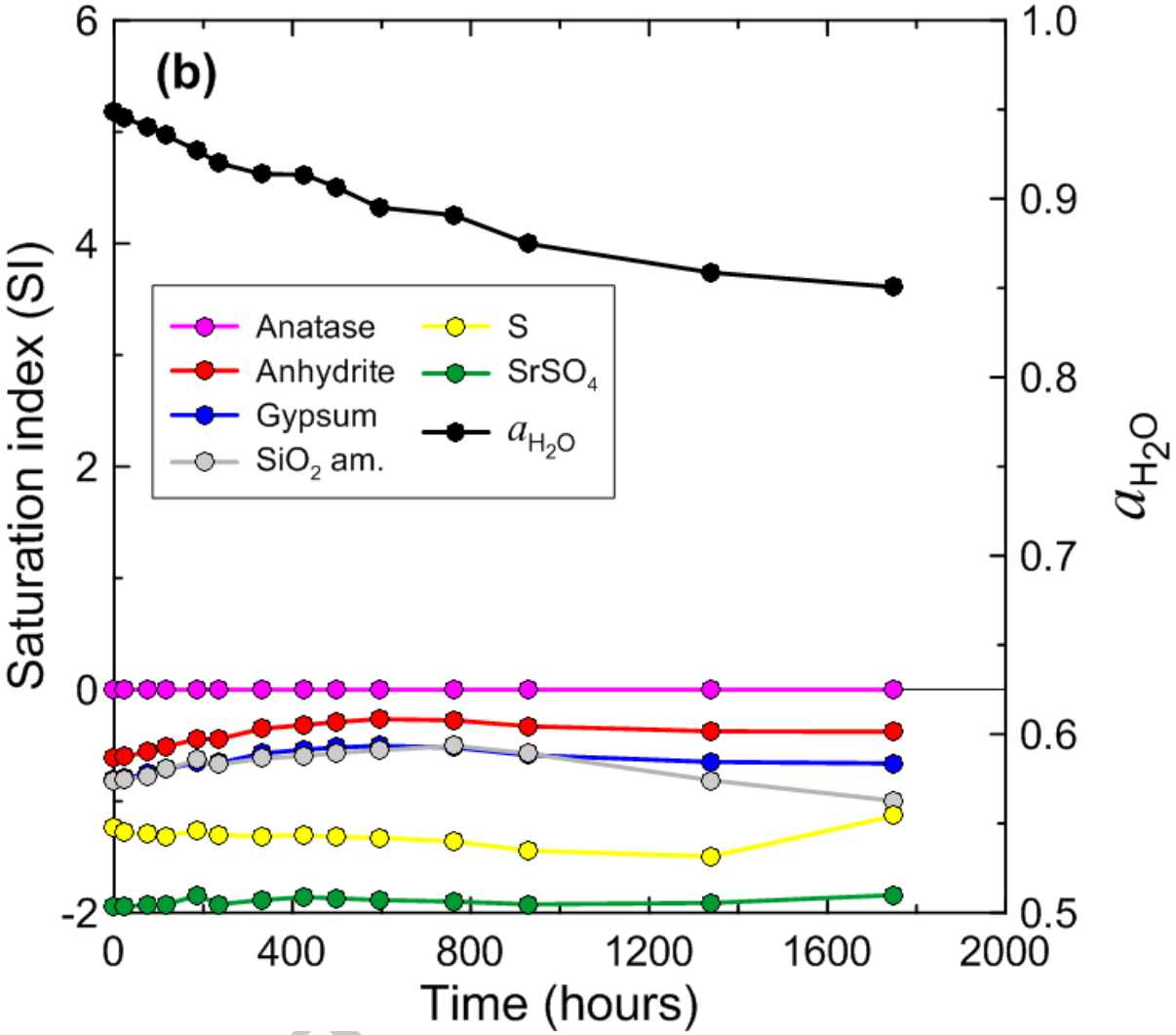

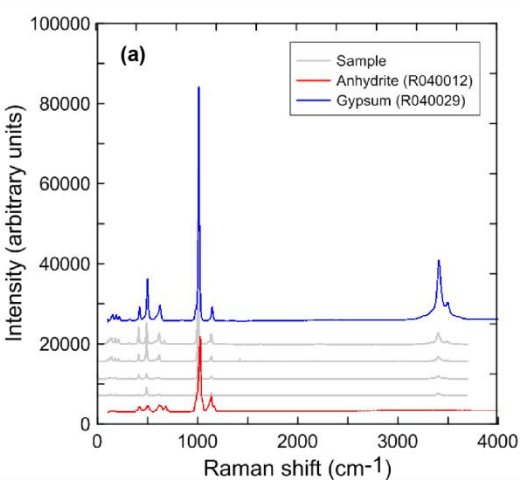

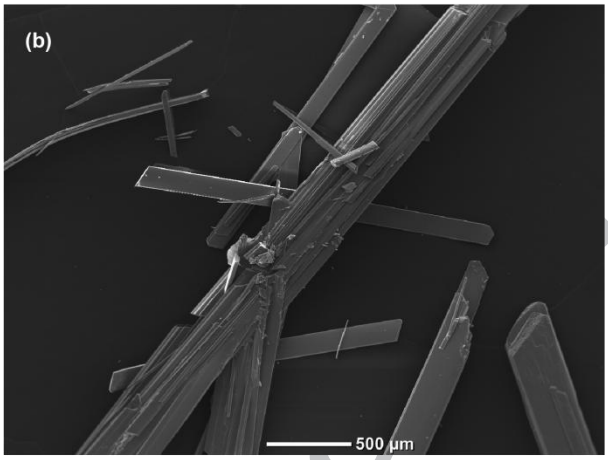

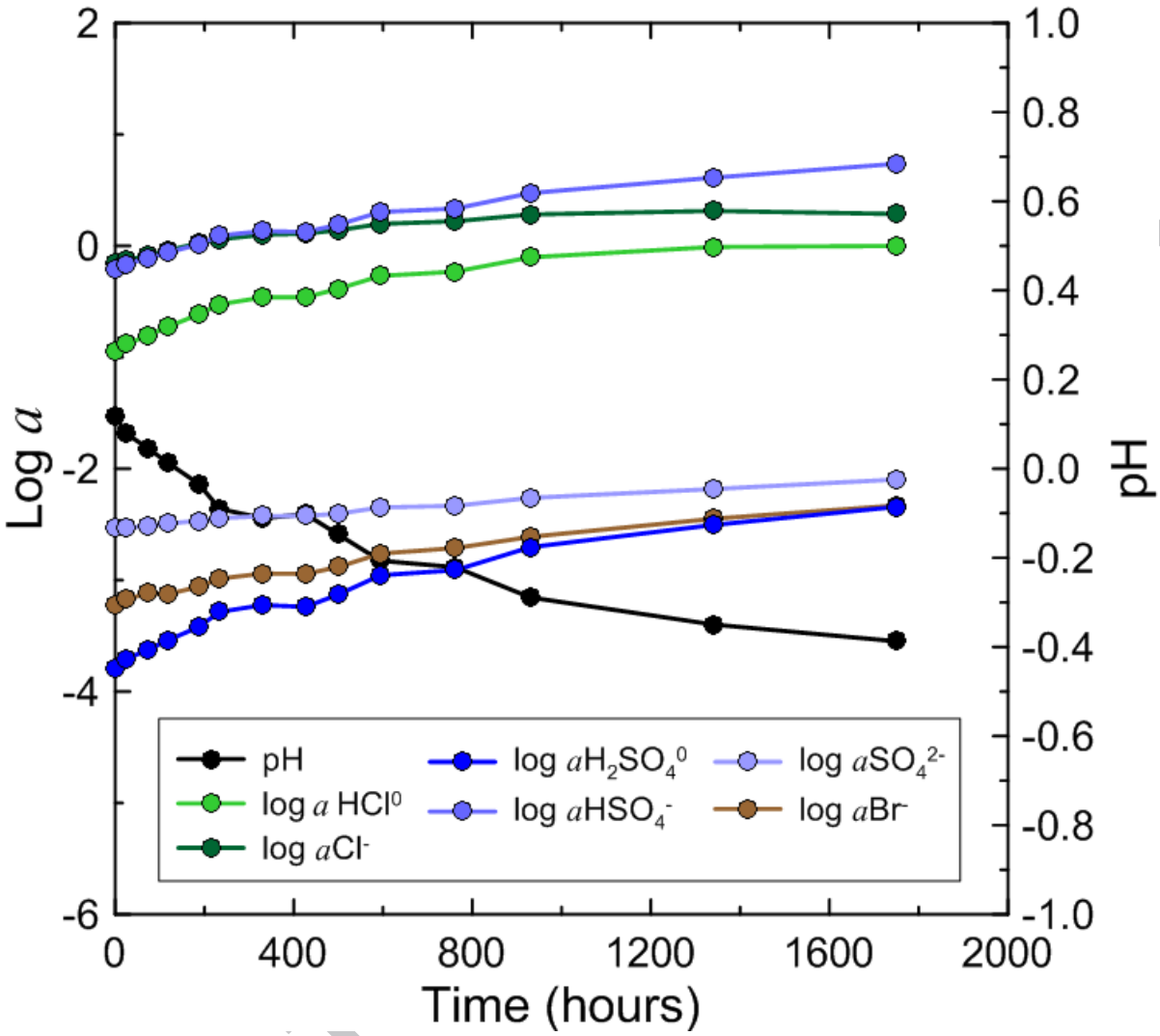
Log a
pH
Time (hours)
2
0
-2
-4
-6
1.0
0.8
0.6
0.4
0.2
0.0
-0.2
-0.4
-0.6
-0.8
-1.0
0
400
800
1200
1600
2000
pH
log a HCl0
log aCl-
log aH2SO40
log aHSO4-
log aSO42-
log aBr-

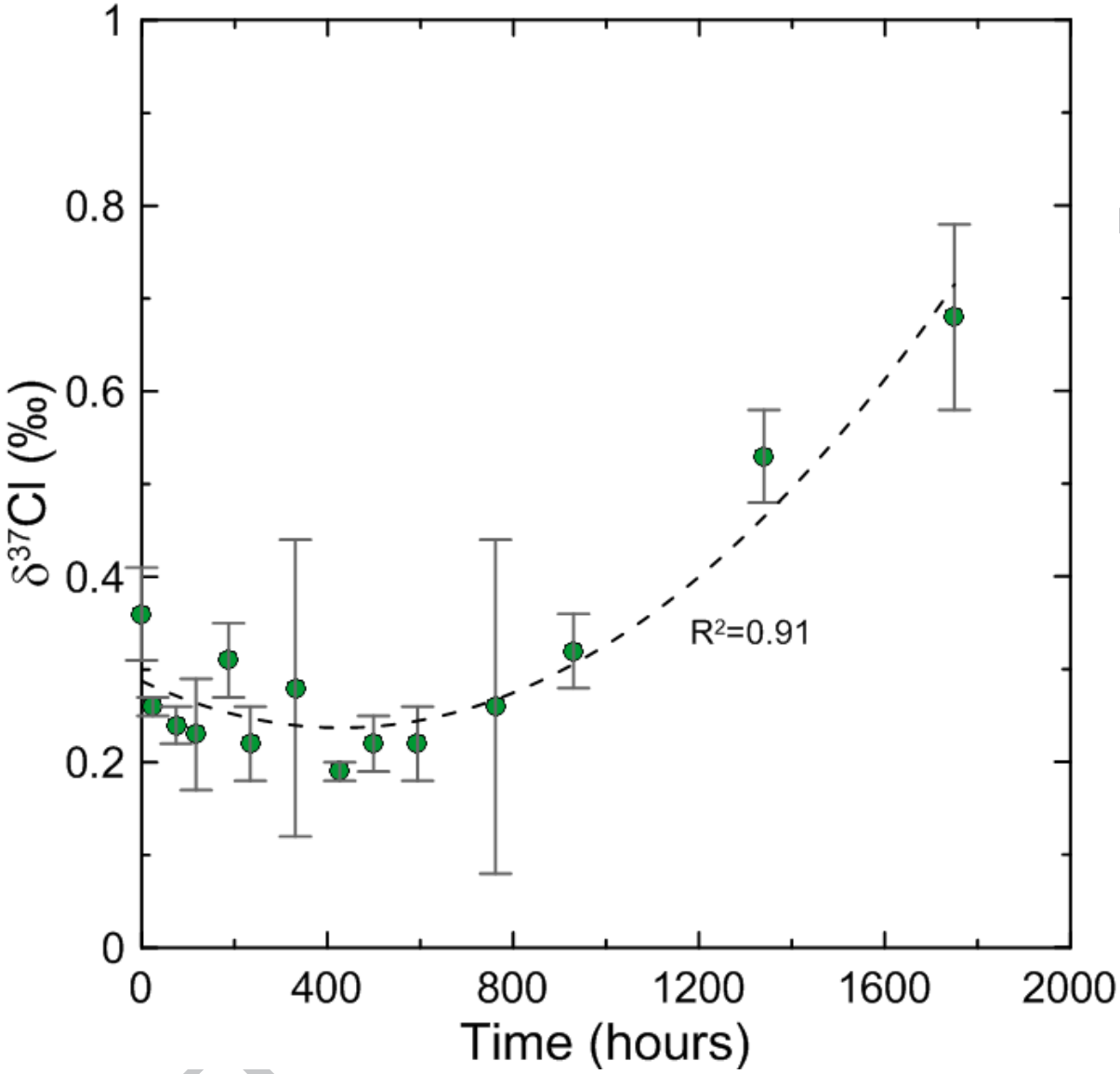

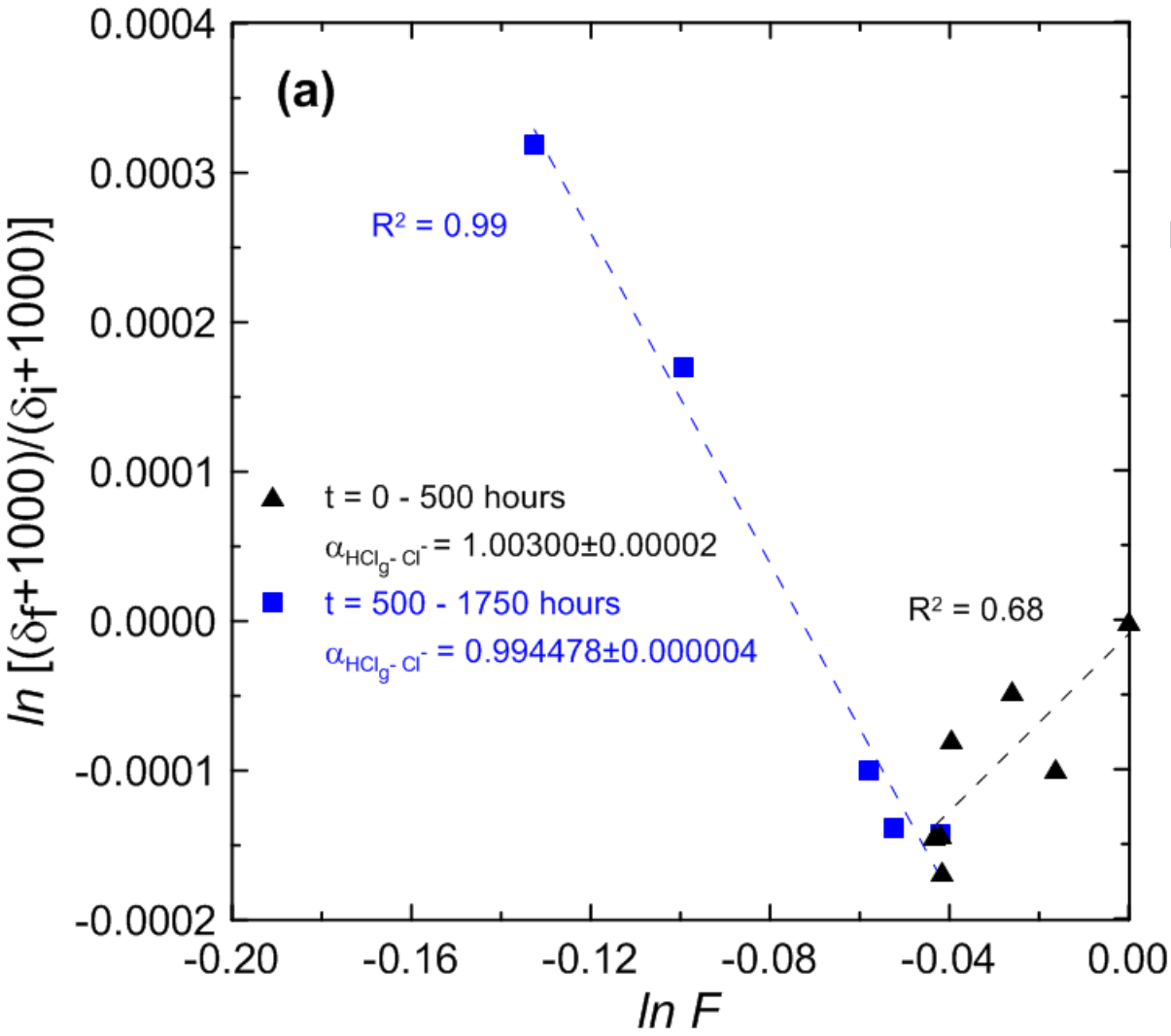
(a)
R² = 0.99
t = 0 - 500 hours
α HClg - Cl- = 1.00300±0.00002
t = 500 - 1750 hours
α HClg - Cl- = 0.994478±0.000004
R² = 0.68
ln [(δf+1000)/(δi+1000)]
ln F
0.0004
0.0003
0.0002
0.0001
0.0000
-0.0001
-0.0002
-0.20
-0.16
-0.12
-0.08
-0.04
0.00

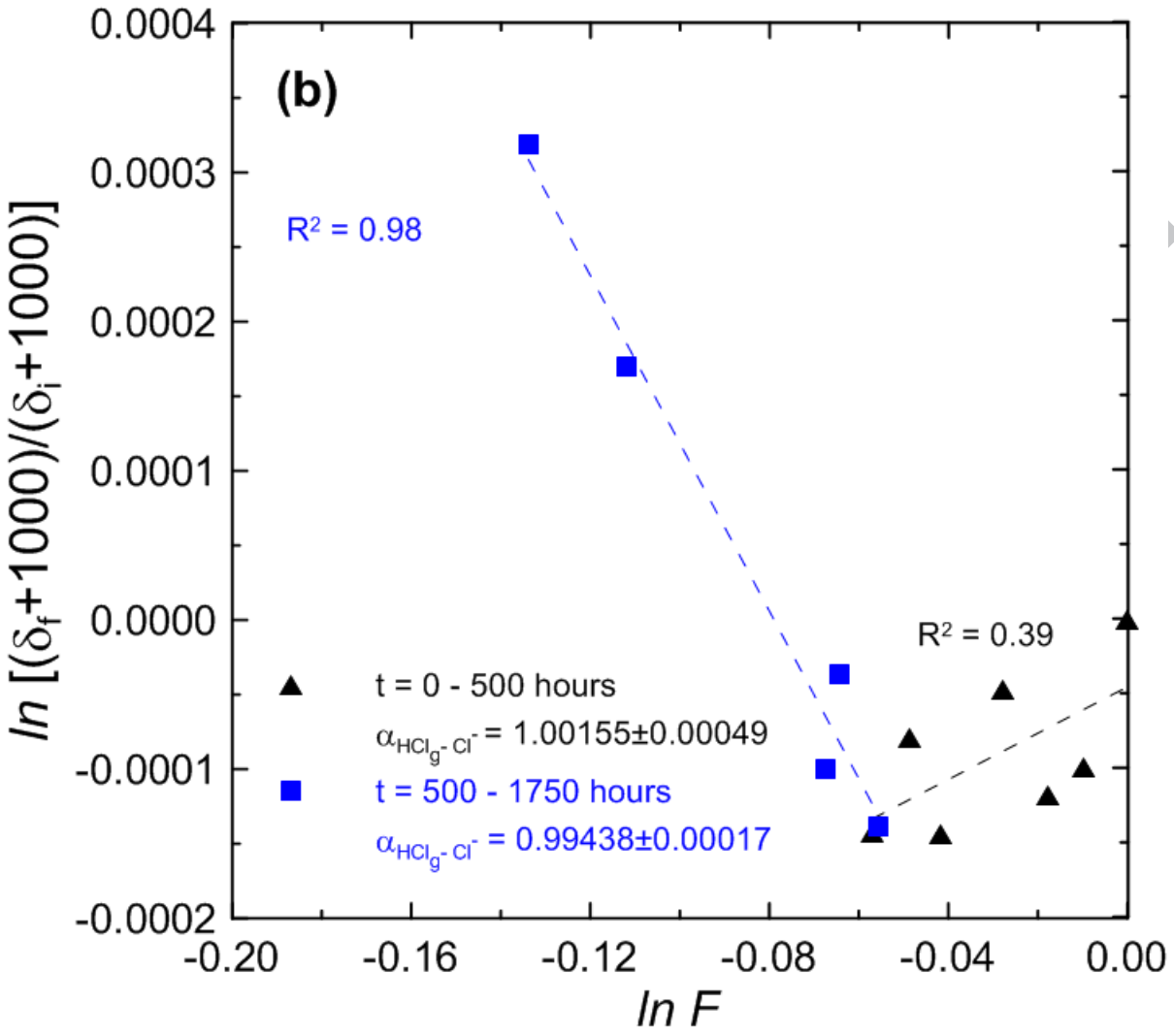
(b)
R² = 0.98
R² = 0.39
t = 0 - 500 hours
$\alpha_{HCl_g\text{-}Cl^-}$ = 1.00155±0.00049
t = 500 - 1750 hours
$\alpha_{HCl_g\text{-}Cl^-}$ = 0.99438±0.00017
ln [(δf+1000)/(δi+1000)]
ln F
0.0004
0.0003
0.0002
0.0001
0.0000
-0.0001
-0.0002
-0.20
-0.16
-0.12
-0.08
-0.04
0.00

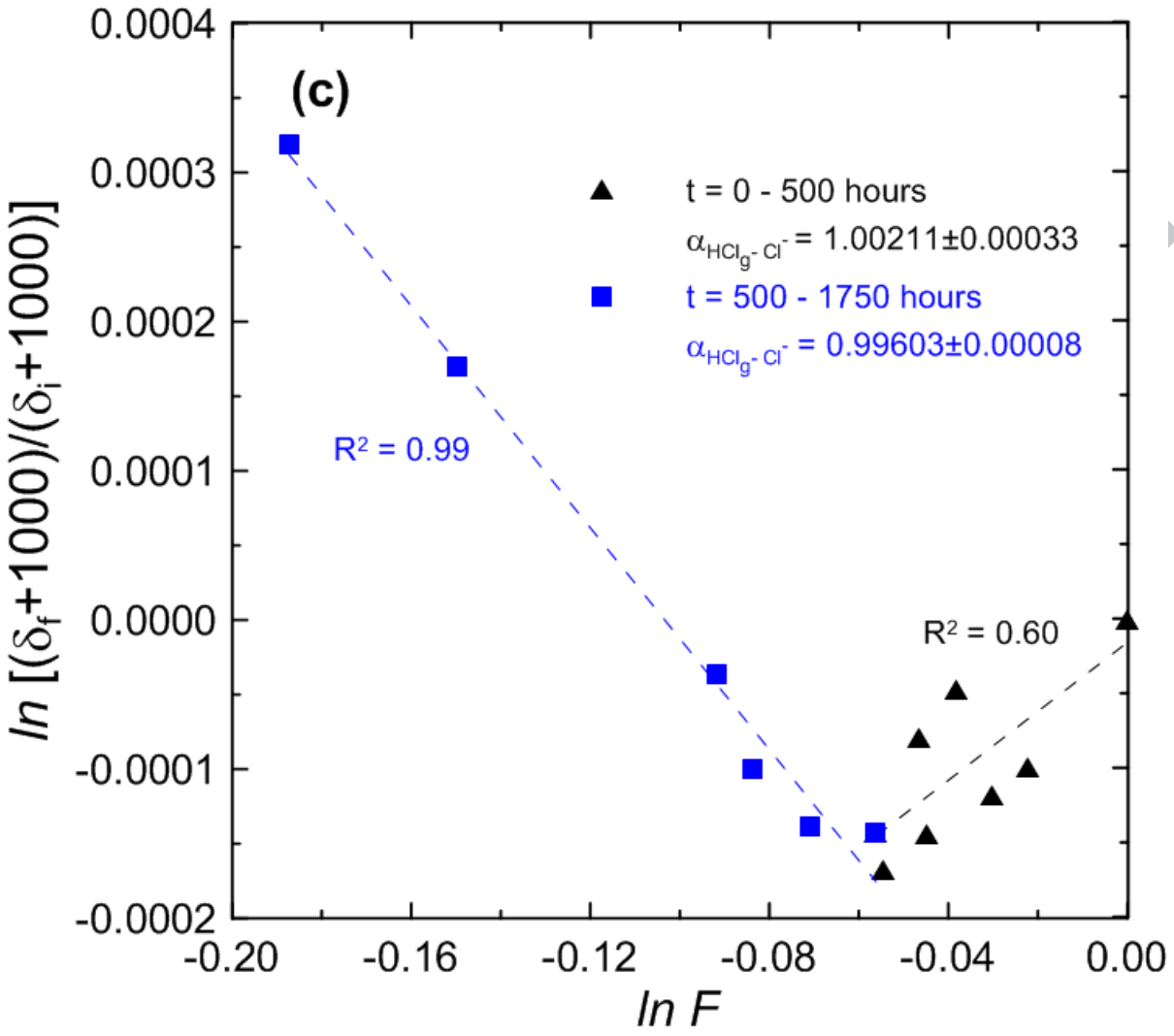
(c)
t = 0 - 500 hours
$\alpha_{HCl_g\text{-}Cl^-}$ = 1.00211±0.00033
t = 500 - 1750 hours
$\alpha_{HCl_g\text{-}Cl^-}$ = 0.99603±0.00008
R² = 0.99
R² = 0.60
ln [(δf+1000)/(δi+1000)]
ln F
0.0004
0.0003
0.0002
0.0001
0.0000
-0.0001
-0.0002
-0.20
-0.16
-0.12
-0.08
-0.04
0.00

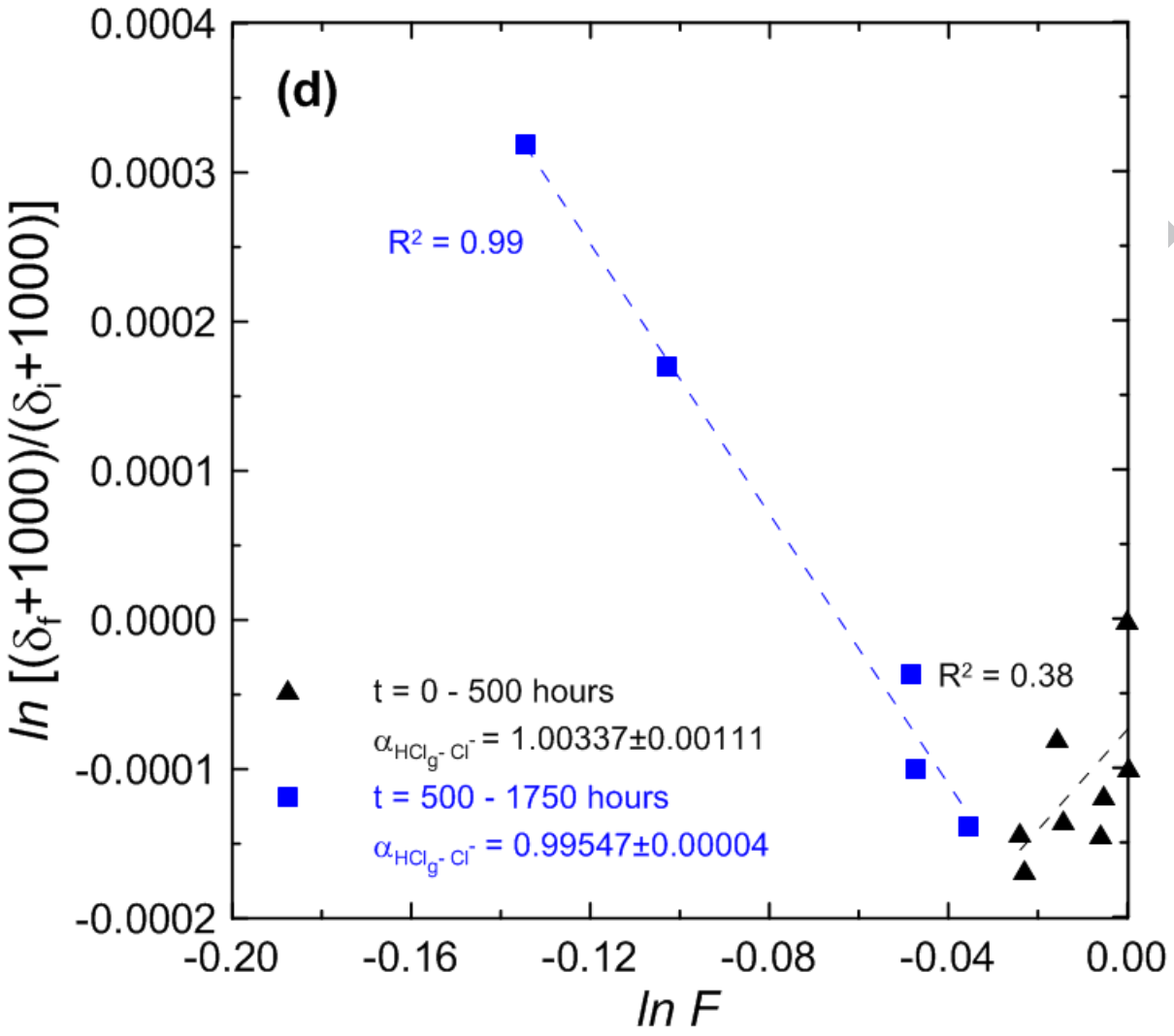
(d)
R² = 0.99
R² = 0.38
t = 0 - 500 hours
$\alpha_{HCl_g\text{-}Cl^-}$ = 1.00337±0.00111
t = 500 - 1750 hours
$\alpha_{HCl_g\text{-}Cl^-}$ = 0.99547±0.00004
ln [(δf+1000)/(δi+1000)]
ln F
0.0004
0.0003
0.0002
0.0001
0.0000
-0.0001
-0.0002
-0.20
-0.16
-0.12
-0.08
-0.04
0.00

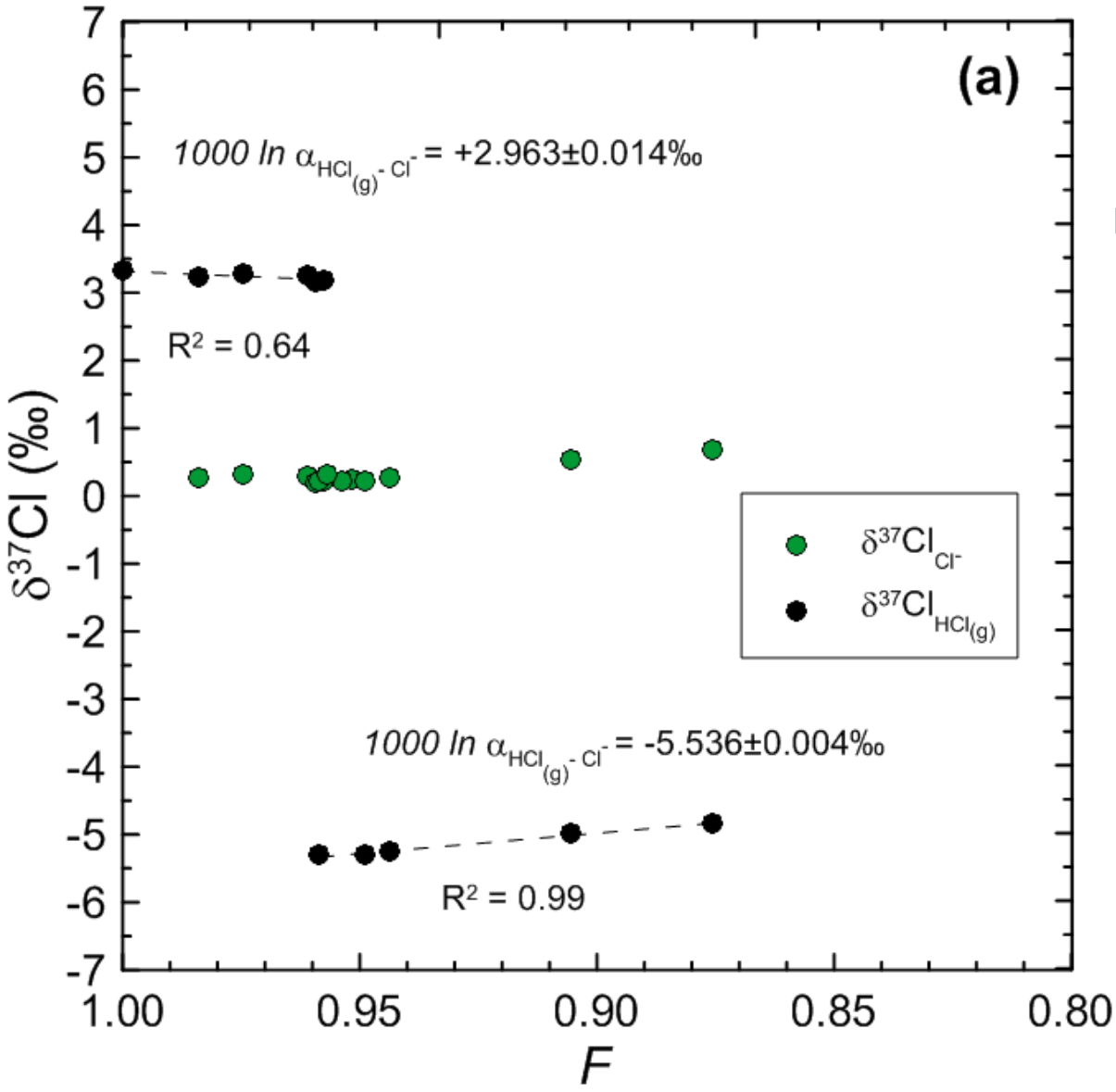
(a)
1000 ln α HCl(g)- Cl- = +2.963±0.014‰
R² = 0.64
1000 ln α HCl(g)- Cl- = -5.536±0.004‰
R² = 0.99
δ37Cl Cl-
δ37Cl HCl(g)
δ37Cl (‰)
F
7
6
5
4
3
2
1
0
-1
-2
-3
-4
-5
-6
-7
1.00
0.95
0.90
0.85
0.80

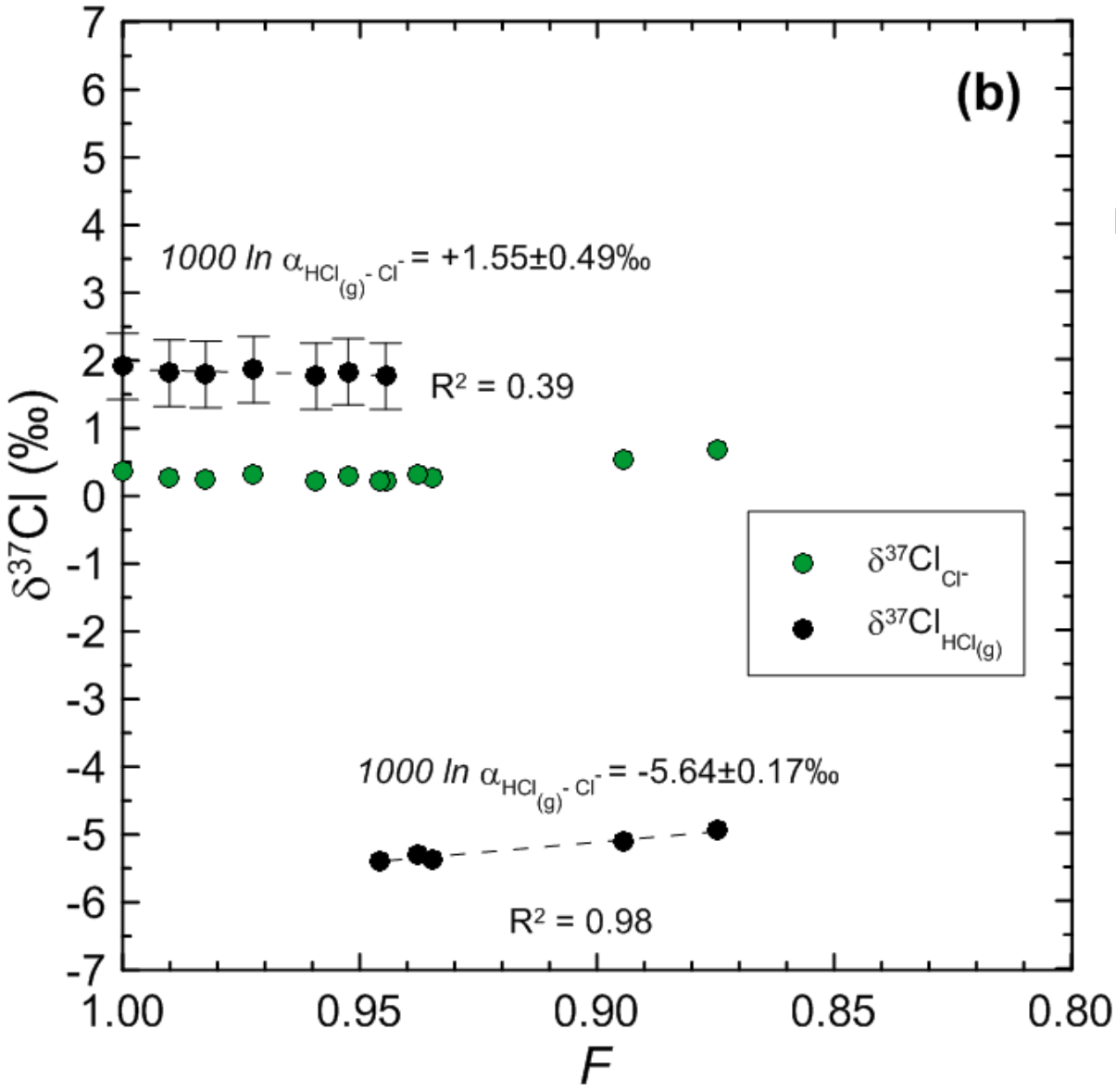
(b)
1000 ln α HCl(g)- Cl- = +1.55±0.49‰
R² = 0.39
δ37Cl Cl-
δ37Cl HCl(g)
1000 ln α HCl(g)- Cl- = -5.64±0.17‰
R² = 0.98
δ37Cl (‰)
F
7
6
5
4
3
2
1
0
-1
-2
-3
-4
-5
-6
-7
1.00
0.95
0.90
0.85
0.80

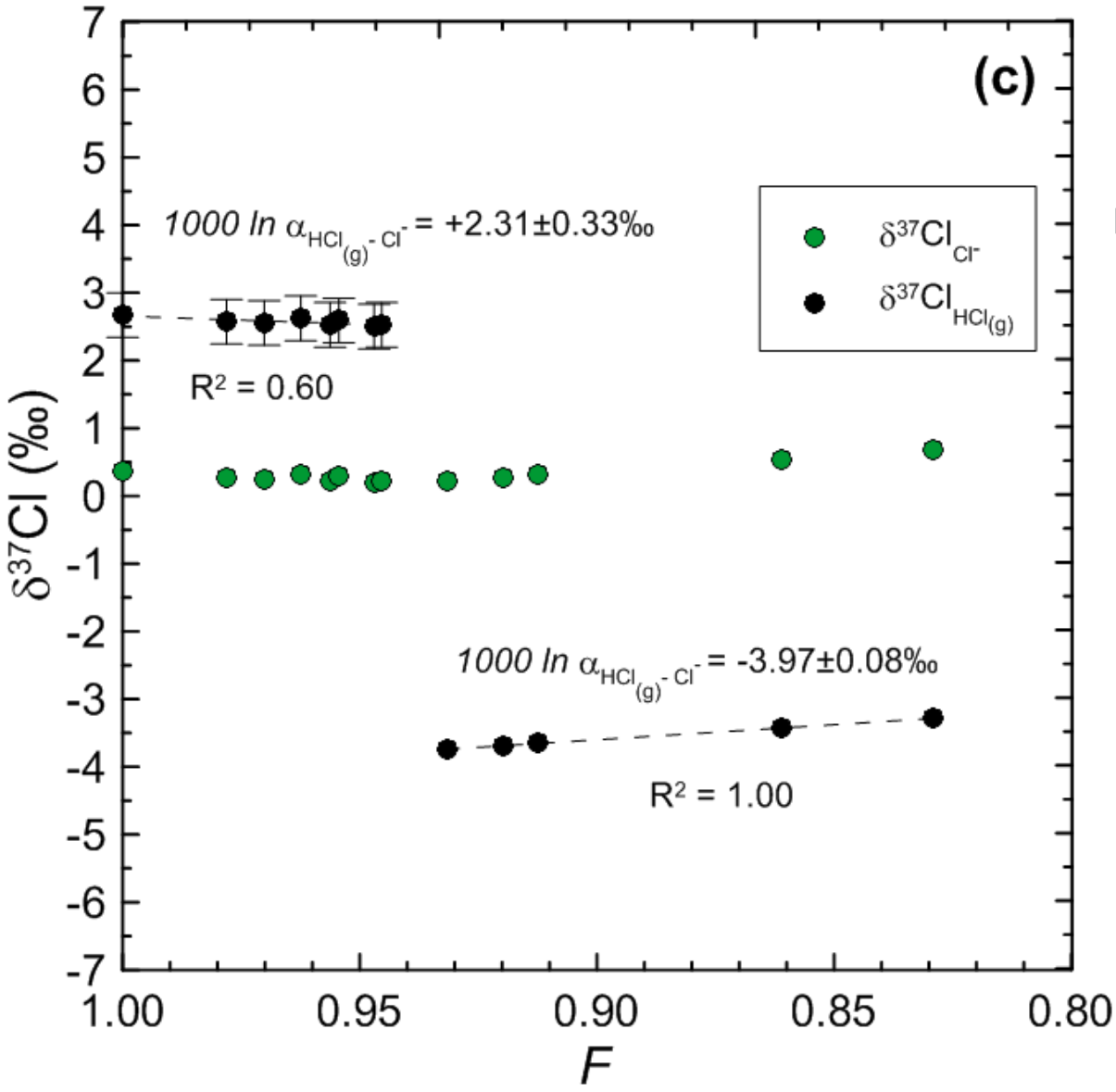
(c)
1000 ln α HCl(g)- Cl- = +2.31±0.33‰
R² = 0.60
1000 ln α HCl(g)- Cl- = -3.97±0.08‰
R² = 1.00
δ37Cl Cl-
δ37Cl HCl(g)
δ37Cl (‰)
F
7
6
5
4
3
2
1
0
-1
-2
-3
-4
-5
-6
-7
1.00
0.95
0.90
0.85
0.80

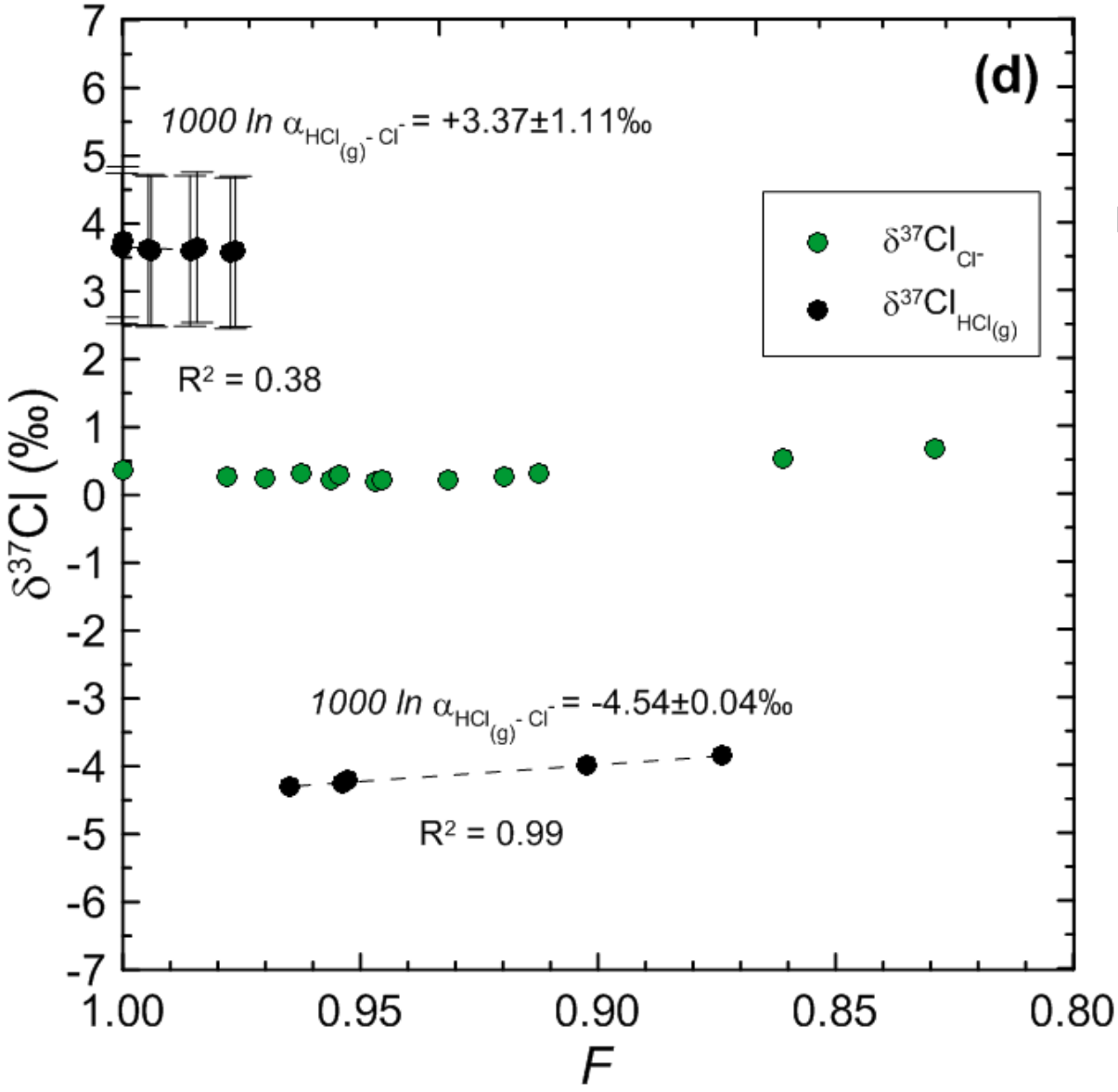
(d)
1000 ln $\alpha_{HCl_{(g)}\text{-}Cl^-}$ = +3.37±1.11‰
$\delta^{37}Cl_{Cl^-}$
$\delta^{37}Cl_{HCl(g)}$
R² = 0.38
1000 ln $\alpha_{HCl_{(g)}\text{-}Cl^-}$ = -4.54±0.04‰
R² = 0.99
δ^{37}Cl (‰)
F
7
6
5
4
3
2
1
0
-1
-2
-3
-4
-5
-6
-7
1.00
0.95
0.90
0.85
0.80

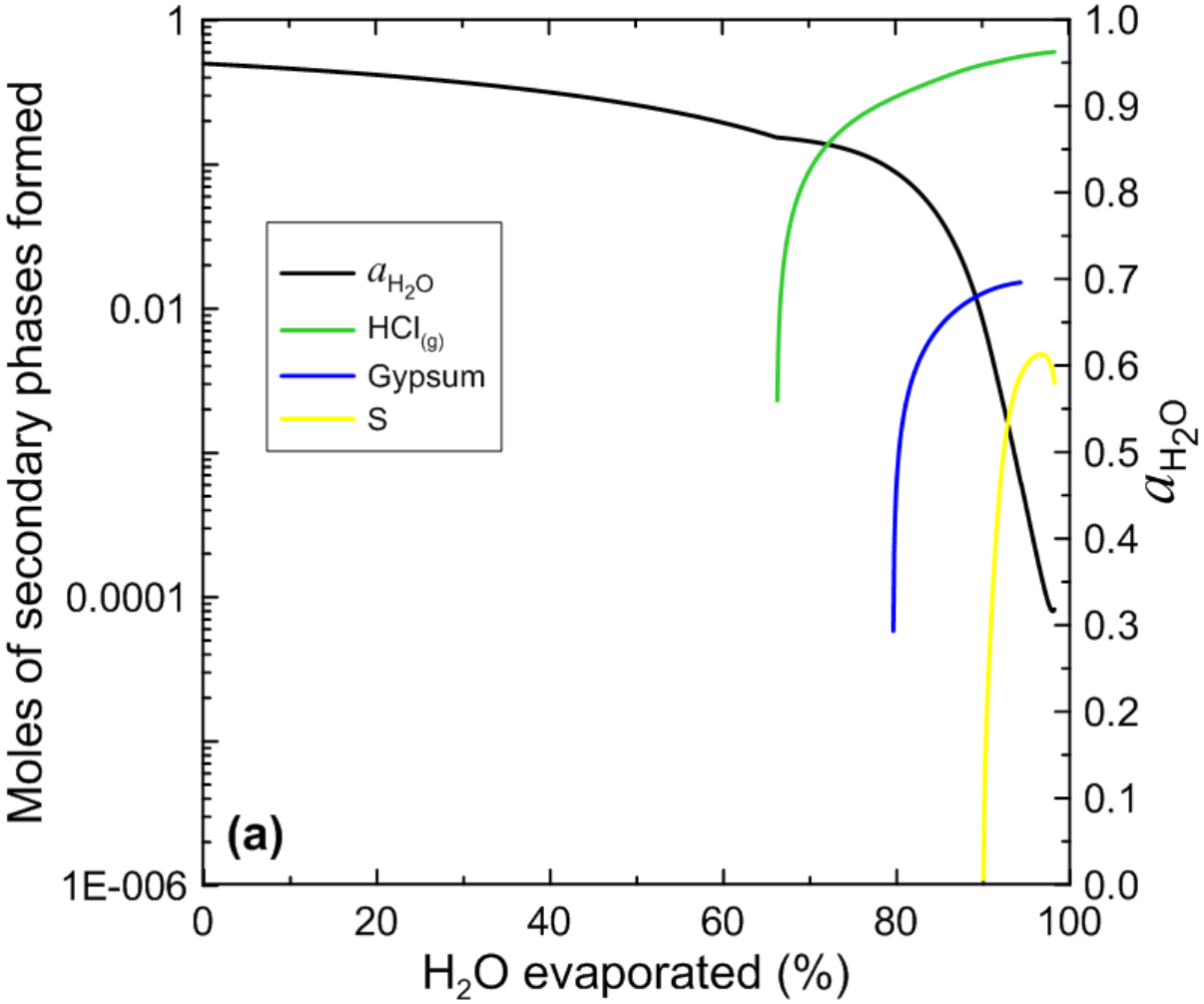
Moles of secondary phases formed
1
0.01
0.0001
1E-006
0
20
40
60
80
100
H2O evaporated (%)
1.0
0.9
0.8
0.7
0.6
0.5
0.4
0.3
0.2
0.1
0.0
aH2O
aH2O
HCl(g)
Gypsum
S
(a)

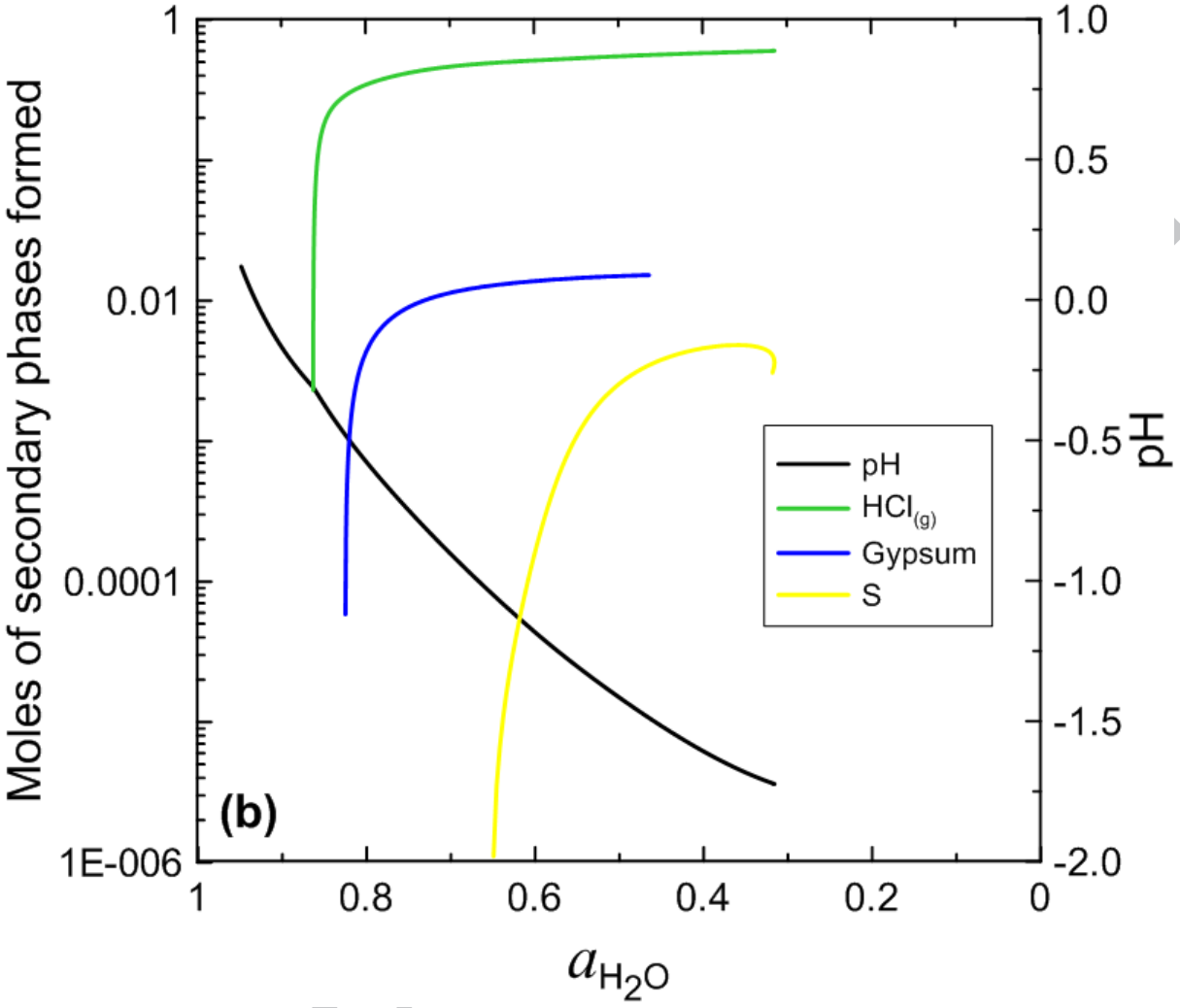

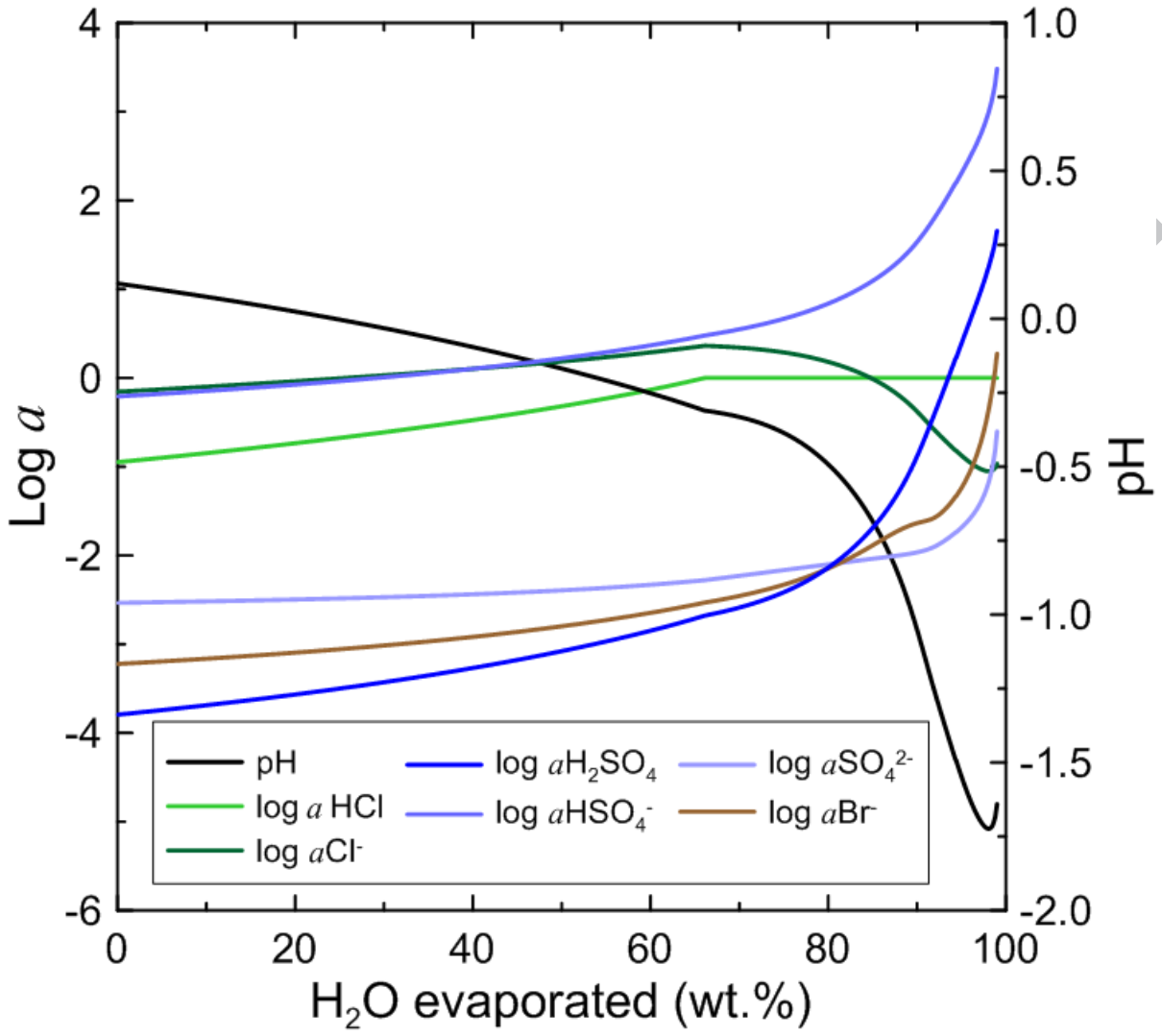
Log a
pH
H2O evaporated (wt.%)
pH
log a HCl
log aCl-
log aH2SO4
log aHSO4-
log aSO4 2-
log aBr-
4
2
0
-2
-4
-6
1.0
0.5
0.0
-0.5
-1.0
-1.5
-2.0
0
20
40
60
80
100

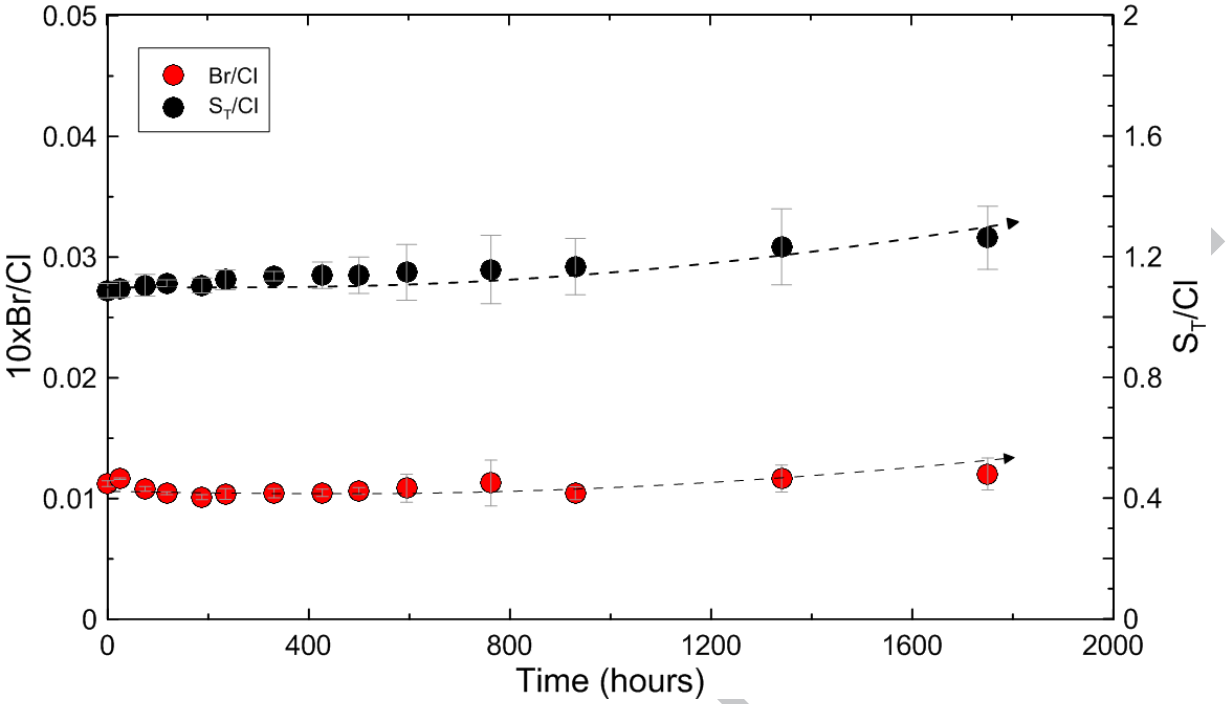

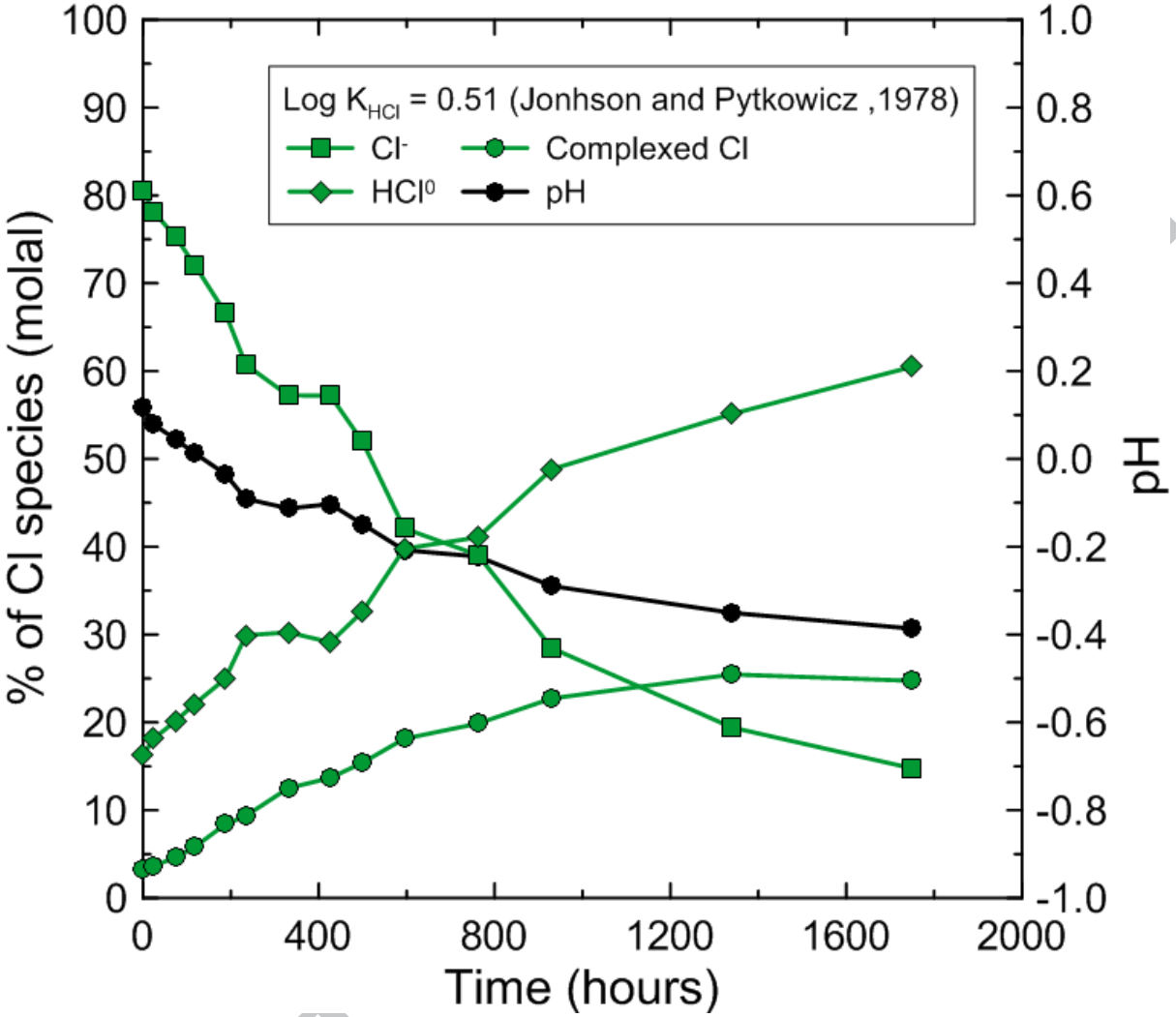
Log K_{HCl} = 0.51 (Jonhson and Pytkowicz ,1978)
Cl-
Complexed Cl
HCl0
pH
% of Cl species (molal)
pH
Time (hours)
0
400
800
1200
1600
2000
0
10
20
30
40
50
60
70
80
90
100
1.0
0.8
0.6
0.4
0.2
0.0
-0.2
-0.4
-0.6
-0.8
-1.0

Sample	Time (hours)	pH (20±1°C)	EC (mS/cm)	$W_{initial}$ (g)	W_{final} (g)	W_{loss} (g)	Evaporation (wt. %)	Evaporation rate (g/h/dm^2)
0	0	0.10	283	n.d.	n.d.	n.d.	n.d.	n.d.
1	24	0.06	288	53.7677	51.0734	2.6944	5.01	1.86
2	74	0.03	308	53.7424	46.1068	7.6356	14.21	1.71
3	117	-0.01	322	53.8037	43.0863	10.7175	19.92	1.52
4	187	-0.05	342	53.7731	44.5965	9.1765	27.52	1.32
5	234	-0.11	351	53.1711	37.0523	16.1189	30.31	1.15
6	331	-0.13	367	53.7166	33.6840	20.0326	37.29	1.01
7	427	-0.12	376	53.6621	32.4211	21.2410	39.58	0.83
8	500	-0.16	383	53.7552	30.9041	22.8511	42.51	0.76
9	594	-0.22	390	53.7663	28.9339	24.8324	46.19	0.70
10	762	-0.24	395	53.7697	27.5417	26.2281	48.78	0.57
11	930	-0.31	401	53.7009	25.3190	28.3819	52.85	0.51
12	1340	-0.37	397	53.7580	22.5509	31.2071	58.05	0.39
13	1750	-0.41	392	53.6935	22.6709	31.0226	57.78	0.29

Sample	Time	pH	S_T[a]	Cl	F	Al	B	Br	Ca	Fe	K	Mg	Na	Si	Sr	Ti	TDS[b]
	(hours)	(20±1°C)	(mg/kg)	(mg/kg)	(mg/kg)	(mg/kg)	(mg/kg)	(mg/kg)	(mg/kg)	(mg/kg)	(mg/kg)	(mg/kg)	(mg/kg)	(mg/kg)	(mg/kg)	(mg/kg)	(g/kg)
0[c]	0	0.10	21800	22100	1410	5730	49	56	690	1970	1230	690	1110	32	15	7.1	96
1	24	0.06	22600	22900	1500	5920	51	60	730	2080	1270	710	1150	33	15	7.4	100
2	74	0.03	24500	24500	1570	6400	55	60	790	2250	1370	770	1240	35	17	8.2	111
3	117	-0.01	26500	26300	1710	6970	61	62	860	2450	1490	830	1340	38	18	9.0	119
4	187	-0.05	29700	29700	1900	7790	68	68	960	2750	1660	920	1510	42	20	10.3	137
5	234	-0.11	30900	30400	1880	8010	70	71	990	2830	1710	950	1540	43	21	10.6	142
6	331	-0.13	34800	33900	2240	8970	79	80	1110	3160	1910	1070	1730	48	23	12.1	160
7	427	-0.12	36200	35100	2260	9340	81	83	1150	3300	1990	1120	1800	50	24	12.7	166
8	500	-0.16	38000	36900	2400	9820	87	88	1220	3470	2100	1180	1890	53	25	13.4	174
9	594	-0.22	40500	39000	2440	10500	91	95	1300	3720	2240	1260	2000	56	27	14.4	185
10	762	-0.24	42700	40700	2640	11200	97	104	1230	3940	2360	1330	2110	60	27	15.2	195
11	930	-0.31	47400	44900	2980	12500	106	106	1000	4380	2620	1470	2330	66	28	17.0	214
12	1340	-0.37	53200	47700	3340	14000	118	125	790	4930	2960	1650	2630	70	31	19.1	239
13	1750	-0.41	52400	45900	3110	13800	116	124	700	4920	2920	1630	2610	55	29	19.0	234

Notes: (a) total sulphur, measured by ICP-OES; (b) calculated total dissolved solids; (c) the chemical composition of the sample 0 (t=0 hours) was extrapolated based on the analyses of the consecutive samples.

Sample	Time (hours)	Evaporation (wt.%)	pH (20±1°C)	$\delta^{37}Cl_{Cl\ diss.}$ (‰)	$Cl_{measured}$ (mg/kg)	$Cl_{calculated}$ (mg/kg)	Cl_{loss} (mg/kg)	Cl_{loss} (mg)	$Cl_{initial}$ (mg)	*F*	*ln F*	$ln((\delta_f + 1000)/(\delta_i + 1000))$	$1000*ln(\alpha_{HCl\ (g)\ -\ Cl\ diss.})$	$\delta^{37}Cl_{HCl\ (g)}$
0	0	0.00	0.10	+0.36±0.05	22100	22100	0	0		1.00	0.0000	0	+2.963±0.014	+3.327±0.014
1	24	5.01	0.06	+0.26±0.01	22900	23300	370	20	1190	0.98	-0.0162	-9.8719E-05		+3.229±0.014
2	74	14.21	0.03	+0.24±0.02	24500	25800	1250	60	1190					
3	117	19.92	-0.01	+0.22±0.06	26300	27600	1270	50	1190					
4	187	27.52	-0.05	+0.31±0.04	29700	30500	780	30	1190	0.97	-0.0259	-4.6734E-05		+3.281±0.014
5	234	30.31	-0.11	+0.22±0.04	30400	31700	1350	50	1180	0.96	-0.0434	-1.4371E-04		+3.184±0.014
6	331	37.29	-0.13	+0.28±0.16	33900	35300	1370	50	1190	0.96	-0.0396	-7.9604E-05		+3.248±0.014
7	427	39.58	-0.12	+0.19±0.01	35100	36600	1490	50	1190	0.96	-0.0415	-1.6770E-04		+3.160±0.014
8	500	42.51	-0.16	+0.22±0.03	36900	38500	1590	50	1190	0.96	-0.0421	-1.4321E-04	-5.536±0.004	-5.304±0.004
9	594	46.19	-0.22	+0.22±0.04	39000	41100	2100	60	1190	0.95	-0.0525	-1.3871E-04		-5.300±0.004
10	762	48.78	-0.24	+0.26±0.18	40700	43200	2440	70	1190	0.94	-0.058	-9.9598E		-5.261±0.004

											0	-05		
11	930	52.85	-0.31	+0.32±0.04	44900	46900	2020	50	1190					
12	1340	58.05	-0.37	+0.53±0.05	47700	52700	4990	110	1190	0.91	-0.0993	1.7017E-04		-4.991±0.004
13	1750	57.78	-0.41	+0.68±0.05	45900	52400	6510	150	1190	0.88	-0.1326	3.1908E-04		-4.842±0.004

Method	t = 0 - 500 h		t = 500 - 1750 h	
	$\alpha_{HCl\ (g)\ -\ Cl\ diss.}$	$1000*ln(\alpha_{HCl\ (g)\ -\ Cl\ diss.})$	$\alpha_{HCl\ (g)\ -\ Cl\ diss.}$	$1000*ln(\alpha_{HCl\ (g)\ -\ Cl\ diss.})$
Cl independent mass loss	1.00300±0.000002	+2.963±0.014‰	0.994479±0.000004	-5.536±0.004‰
Cl/B	1.00155±0.00049	+1.55±0.49‰	0.99438±0.00017	-5.64±0.17‰
Cl/Fe	1.00211±0.00033	+2.31±0.33‰	0.99603±0.00008	-3.97±0.08‰
Cl/Mg	1.00337±0.00111	+3.37±1.11‰	0.99547±0.00004	-4.54±0.04‰